European Journal of Pharmaceutical Sciences 213 (2025) 107216

Contents lists available at ScienceDirect

European Journal of Pharmaceutical Sciences

journal homepage: www.elsevier.com/locate/ejps

Microfluidic-assisted synthesis of integrin-targeting cRGD liposomes as a scalable strategy for theranostic applications in triple-negative breast cancer

Karina Ovejero-Paredes [a,b,c,1], Giovanni Bisbano [d,1], Inge Flier [a,e], Alejandro González-Simón [a], Marzia Marciello [a,b,f], Sabrina Oliveira [e,g], Marco Zupi [d], Davide Rubes [d], Fatima Ayash [a,d], Filippo Doria [h], Valentina Pirota [h], Marco Terreni [d], Massimo Serra [d,**], Marco Filice [a,b,f,*]

[a] Nanobiotechnology for Life Sciences Group, Department of Chemistry in Pharmaceutical Sciences, Faculty of Pharmacy, Universidad Complutense de Madrid (UCM), Plaza Ramón y Cajal s/n, Madrid E-28040, Spain
[b] Microscopy and Dynamic Imaging Unit, Fundación Centro Nacional de Investigaciones Cardiovasculares Carlos III (CNIC), Calle Melchor Fernandez Almagro 3, Madrid E-28029, Spain
[c] Research Unit of Intelligent Technology for Health and Wellbeing, Department of Engineering, Università Campus Bio-Medico di Roma, Via Alvaro del Portillo, 21, Rome 00128, Italy
[d] Department of Drug Sciences, University of Pavia, Viale Taramelli 12, Pavia, PV 27100, Italy
[e] Department of Pharmaceutics, Utrecht Institute for Pharmaceutical Sciences, Utrecht University, Utrecht 3584 CG, the Netherlands
[f] 12 de Octubre Health Research Institute (imas12), Madrid 28041, Spain
[g] Department of Biology, Utrecht University, Utrecht 3584 CH, the Netherlands
[h] Department of Chemistry, University of Pavia, Viale Taramelli 10, Pavia, PV 27100, Italy

ARTICLE INFO

Keywords:
Liposome
Nanomedicine
cRGD
Integrins
Anticancer
Microfluidic
Triple-negative breast cancer
Drug delivery
Theranosis
Precision medicine
Nanobiotechnology
Cell spheroids
3D in vitro models

ABSTRACT

Triple negative breast cancer (TNBC) represents one of the most aggressive types of cancer, with a difficult treatment leading to poor prognosis of the disease. Herein we report the synthesis of a custom-made cyclic RGD peptide (cRGD), and its use in decorating liposomes for targeted drug delivery of doxorubicin to TNBC cells overexpressing integrin receptor $\alpha_v\beta_3$. Liposomes carrying dibenzocyclooctine groups on their surface were produced using an optimized large scale microfluidic-assisted approach and subsequently conjugated with cRGD bearing an acyl azide group by means of a click chemistry reaction. This functionalization promotes enhanced cellular uptake via integrin-mediated endocytosis. *In vitro* assessments confirm enhanced selectivity and cytotoxicity of cRGD-liposomes against triple-negative cancer cells, in addition to dual imaging capabilities by fluorescence and magnetic resonance techniques due to the incorporation of a fluorescent dye and gadolinium complex, respectively. These features support the potential of cRGD-liposomes as a promising platform for targeted drug delivery to specific cancer cell populations, establishing them as viable theranostic agents for precision medicine applications.

1. Introduction

Cancer poses a remarkable challenge to global health. Among its various forms, breast cancer remains a significant contributor to cancer-related morbidity and mortality, especially for women (Lee et al., 2019; Bray et al., 2018; Sanchez-Collado et al., 2019). A particularly aggressive subtype is Triple Negative Breast Cancer (TNBC) (Bianchini et al., 2016), which lacks expression of estrogen receptor, progesterone

* Corresponding author at: Nanobiotechnology for Life Sciences Group, Department of Chemistry in Pharmaceutical Sciences, Faculty of Pharmacy, Universidad Complutense de Madrid (UCM), Plaza Ramón y Cajal s/n, Madrid E-28040, Spain.
** Corresponding author.
E-mail addresses: massimo.serra@unipv.it (M. Serra), mfilice@ucm.es (M. Filice).
[1] These authors contributed equally to this work.

https://doi.org/10.1016/j.ejps.2025.107216
Received 8 May 2025; Received in revised form 13 July 2025; Accepted 22 July 2025
Available online 23 July 2025

receptor, and human epidermal growth factor receptor 2 (HER2). TNBC accounts for a disproportionately high number of breast cancer-related deaths due to its aggressive nature, limited therapeutic options, and higher rates of recurrence (Lee et al., 2019; Ramadan et al., 2018; Mustacchi and De Laurentiis, 2015; Liedtke et al., 2008; Thomas et al., 2007).

The current therapeutic landscape for TNBC primarily involves surgical interventions, often complemented by radiation therapy at the local level and systemic chemotherapy to address distant metastases. The standard neoadjuvant chemotherapy regimen for TNBC typically employs anthracycline-cyclophosphamide-taxane combinations, demonstrating effectiveness in inducing pathological complete responses. However, the significant toxicity associated with these chemotherapeutic agents poses a substantial challenge, as adverse side effects remain a major drawback of such treatments (Martin et al., 2021; Won and Spruck, 2020).

Among anthracycline treatments, doxorubicin-based chemotherapy stands out as the most frequently used approach for TNBC. This regimen works by inhibiting cancer cell proliferation through the proteolytic activation of a key transcription factor. Despite its efficacy, doxorubicin (DOX) treatments present noteworthy disadvantages, with cardiotoxicity and a low response rate standing out as primary concerns (Thorn et al., 2011). The lack of a specific biomarker for identifying TNBC cells adds to the challenges of DOX therapy, complicating targeted treatment approaches and reducing efficacy (Denard et al., 2018).

To overcome these drawbacks, the strategic encapsulation of drugs within nanoparticles engineered for targeted delivery has emerged as a promising strategy in nanomedicine. This approach complements medicinal chemistry in the development of new anticancer therapies, utilizing both novel and established anticancer drugs (Gomes et al., 2008; Gomes et al., 2013; Kranz and Bodmeier, 2007; Paredes et al., 2020; Ovejero-Paredes et al., 2022). Among the diverse array of nanoparticle options, liposomes have garnered extensive attention as carriers for various agents since the 1960s. A notable advantage lies in their versatility to accommodate both hydrophilic and hydrophobic drugs, encapsulating them within the internal core or incorporating them into the membrane (Saiz et al., 2024).

On this direction, the encapsulation of anthracyclines within liposomes has proven to be a transformative approach (Nogueira et al., 2015). Notably, liposome-encapsulated doxorubicin formulations have demonstrated their clinical utility, exhibiting comparable efficacy with conventional anthracyclines but with reduced toxicity (Wang et al., 2008; Plati et al., 2011). Currently, three formulations with liposomal anthracyclines are available (Lao et al., 2013): Myocet (formulated with conventional liposomes), DaunoXome (liposomes with prolonged circulation half-lives) and Caelyx/Doxil (with pegylated liposomes). These medications represent advancements in doxorubicin (or analogues) based therapy, to optimize the therapeutic profile of anthracyclines, enhancing their efficacy while minimizing adverse effects.

However, the most important advancement in cancer therapy can be obtained with the precision medicine based on nanotechnology combined with medicinal chemistry, in order to design a nanoproduct that can be prepared by grafting nanoparticles with targeting moieties specific for overexpressed marker of cancer cells (Marciello et al., 2016; Tian et al., 2022). This approach is poised to become the next frontier in medicinal chemistry and pharmaceutical technology, driving the development of new therapeutic strategies based on pharmaceutical products tailored for precision and/or personalized medicine.

Recently, several molecular targets have been identified on the surface of TNBC cells. Among them, the altered expression of $\alpha_v\beta_3$ integrin receptor make them good candidates to targeted treatments (Hill et al., 2019; Li et al., 2015). Integrins (e.g. $\alpha_v\beta_3$) are critically involved in angiogenesis, metastasis and invasion of solid tumors and are overexpressed on tumor neovasculature during angiogenesis. Therefore, drug-loaded nanomedicine products decorated with ligands targeting these specific receptors are potentially capable of targeting tumors actively.

In this direction, peptides bearing the Arg-Gly-Asp sequence are known as selective integrin ligands and have been widely used for targeted therapy or imaging of various tumors, including breast cancer (Wu et al., 2017). The conformation of the RGD moiety plays a key role in the selectivity of a given ligand towards different RGD-binding integrins. Specifically, cyclic pentapeptides carrying the RGD sequence turned out to be potent antagonists of $\alpha_v\beta_3$ integrin receptor with potential application in anticancer therapy (Serra et al., 2023a). Cilengitide, or [c(RGDfNMeV)], is a cyclic pentapeptide that incorporates the RGD sequence. It has been evaluated as an anticancer drug in approximately 30 different clinical trials (Mas-Moruno et al., 2010), but its development was discontinued due to failures in phase III, where no improvement in overall patient survival was demonstrated (Stupp et al., 2014). Nonetheless, due to their inherently low toxicity to healthy cells and their high selectivity for integrins overexpressed in various cancer types, recent years have witnessed a resurgence of interest in using RGD-based peptides as active targeting moieties for advanced drug delivery systems (Arosio and Casagrande, 2016; Alipour et al., 2020; Battistini et al., 2021).

Our continuous efforts in this field have been focused on the synthesis of proline-derived azabicycloalkane amino acids (Serra et al., 2023b) and their use as intermediate for the preparation of cRGD peptidomimetics, such as 1a-RGD (Scheme 1), a nanomolar inhibitor of αvβ3 integrin receptor. Biological tests showed the ability of 1a-RGD to inhibit cell migration and attachment and to induce anoikis in glioblastoma cell lines (Russo et al., 2012). Furthermore, 1a-RGD is one of the few compounds that demonstrated pure antagonism toward the biological targets even at doses mimicking low plasma concentrations (Paolillo et al., 2018). Recently, a modified version of 1a-RGD has been successfully exploited in the active targeting of silk fibroin nanoparticles (SFNs) towards various tumor cell lines (Bari et al., 2021; Pirota et al., 2023).

In this work, we present the use of a suitably modified cRGD derivative to decorate the surface of liposomes, aiming to achieve active targeting of the theranostic nanosystem towards "difficult-to-treat" tumors, such as TNBC, that overexpress αvβ3 integrin receptors (Scheme 1).

In the last decades many different strategies have been developed and reported in literature to synthesize multifunctional liposomes (Tenchov et al., 2021; Shah et al., 2020). Due to its intrinsic advantages, microfluidic technology has emerged as a promising alternative to traditional methods for large scale liposome preparation. In fact, this approach offers enhanced control over synthetic parameters, enabling precise manipulation and inter-batch enhanced repeatability of particle size, particle distribution, and other physicochemical properties. The ability to fine-tune these features is crucial for optimizing liposomes for various biomedical applications, including drug delivery, diagnostics, and vaccine development. Furthermore, microfluidic devices facilitate scalability from small laboratory settings to large-scale manufacturing, which is a critical consideration when entering clinical trials (Shepherd et al., 2021). Thus, microfluidic techniques hold significant potential for advancing the field of liposome research, improving the efficacy of liposome-based therapies and fostering their translational clinical application (Zhang and Sun, 2021; Mbua et al., 2011).

In this study, the synthesis of a custom-made cRGD derivative functionalized with an azido group, the preparation of liposomes decorated with dibenzocyclooctine moieties, and their conjugation via click chemistry were carried out to investigate a new approach for the therapy of TNBC based on the selective delivery of anticancer agents such as doxorubicin.

For the preparation of the liposomes, following the optimization of different synthetic parameters, a microfluidic process was set up. Then, the targeted empty liposomes were loaded with doxorubicin by optimizing a remote-loading strategy. Subsequently, a strain-promoted azide-alkyne cycloaddition (SPAAC) (Serra et al., 2017) was employed

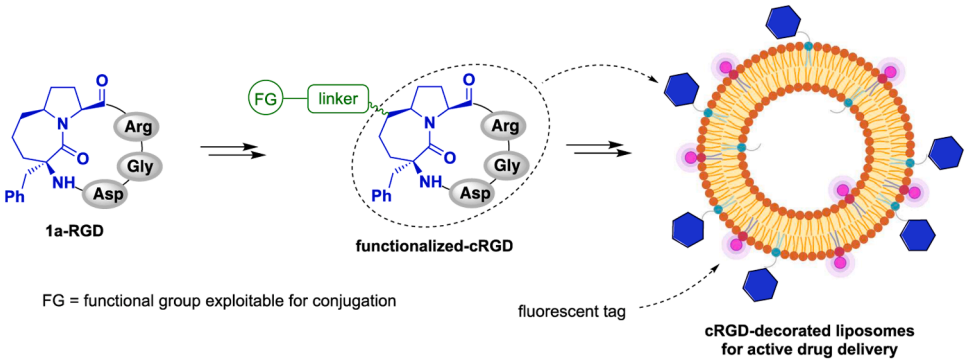

Scheme 1. Decoration of liposomes with cRGDs derivatives.

to decorate the surface of the synthesized liposomes with the aforement azido-cRGD derivative. Finally, the targeting performances and therapeutic efficacy of doxorubicin-loaded cRGD-modified liposomes were evaluated *in vitro* using various cancer cell lines. These included MDA-MB-231 (TNBC), which overexpresses $\alpha_v\beta_3$ integrin receptor, and A375, PANC-1, and MG-63, which do not overexpress these receptors on their surfaces.

2. Results and discussion

2.1. Synthesis of the cRGD directing moiety

The synthesis of the RGD directing moiety involved two steps, i.e. the preparation of a C6-functionalized proline-based azabicycloalkane (Aba) scaffold and the following attachment of the RGD sequence to the scaffold to gain the final RGD-based cyclopentapeptide (cRGD).

2.1.1. Synthesis of the Aba scaffold

To prepare the Aba dipeptide unit we exploited our previously reported synthetic protocol based on a domino cross enyne metathesis/ring closing metathesis (CEYM/RCM) reaction (Serra et al., 2017). The functionalized Aba derivative **3**, carrying a protected amine function on the aryl-ethenyl side chain installed at C6, was straightforwardly achieved by reacting the dipeptide **1** with the styrene derivative **2** in the presence of the Hoveyda-Grubbs catalyst **HG2** (Scheme 2).

The following catalytic hydrogenation of the diene system of **3a** with PtO_2 catalyst allowed the obtainment of **4a** in 91% yield as a single diastereoisomer (for configurational assignment at C6 see Supporting Information).

To arrange the obtained C6-functionalized scaffold **4a** for the incorporation of the RGD sequence, it was submitted to Fmoc cleavage with piperidine, which afforded **5a** in 96% yield.

Due to low stability of **6a** towards chromatographic purification, a one-pot protocol to directly convert **5a** into the corresponding Cbz-protected acid **7a** has been developed. Thus, compound **5a** was first treated with dibenzyl dicarbonate, and then submitted to saponification with LiOH-aqueous methanol at 60 °C for 24 h to gain **7a** in excellent 96% overall yield.

2.1.2. Attachment of the RGD sequence

The in-solution peptide synthesis exploited for the attachment of the RGD sequence, involving as first step the construction of the Arg-Gly unit, has been performed by significantly modifying our previously reported synthetic protocol (Arosio et al., 2008). The Fmoc-protected N^{ω}−2,2,4,6,7-pentamethyldihydrobenzofuran (Pbf)-5-sulfonyl-L-arginine **8** was condensed with glycine methyl ester **9** in the presence of isobutyl chloroformate and N-methylmorpholine (NMM) to give dipeptide **10** (y: 75%, Scheme 3), which was then submitted to cleavage of the Fmoc protecting group affording **11**. The condensation of crude **11** with **7a**, by applying the same reaction conditions as before, allowed,

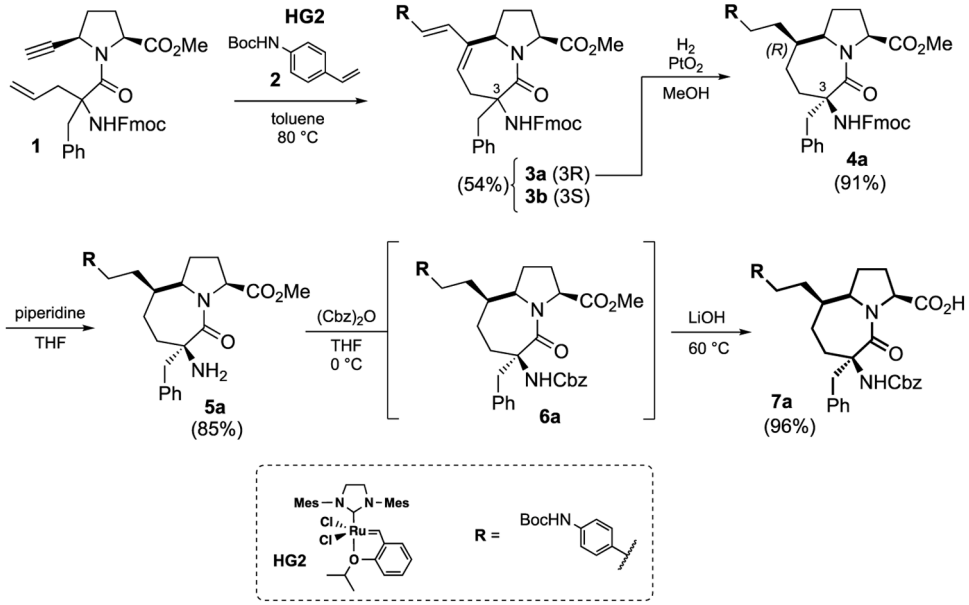

Scheme 2. Synthesis of the C6 functionalized Aba scaffold.

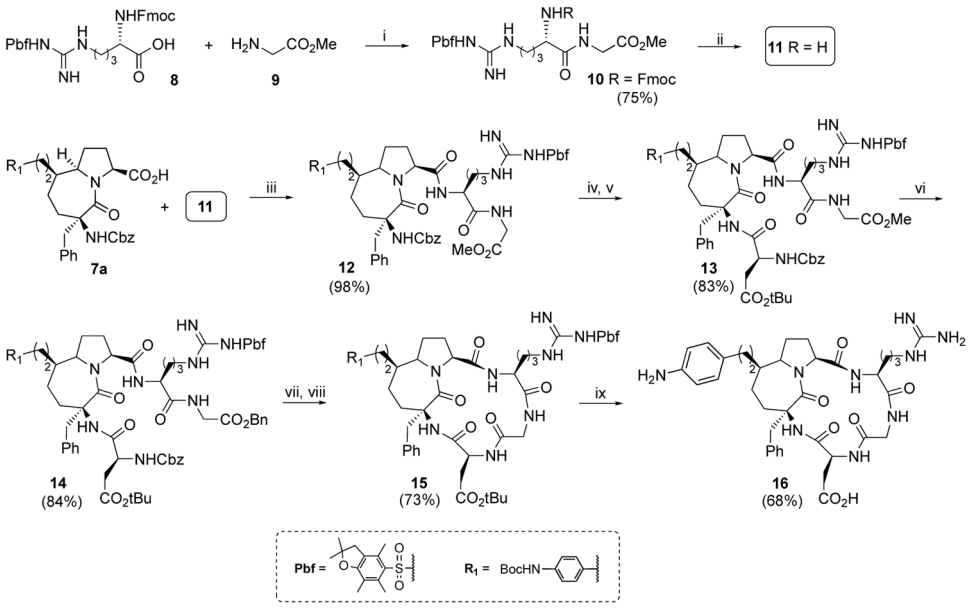

Scheme 3. Reagents and conditions: i) NMM, iBuOCOCl, THF, −30°→ rt, (y: 75%); ii) piperidine, THF (y: 82%). iii) HATU, THF, rt (y: 98%); iv) H_2, $Pd(OH)_2$/C, MeOH; v) Z-Asp(OtBu)-OH, HATU, DIPEA, THF, rt (2 steps, y: 83%); vi) BnOH, $Ti(iPrO)_4$, THF, 90 °C (y: 84%); vii) H_2, $Pd(OH)_2$/C, MeOH; viii) HATU, DIPEA, THF (2 steps, y: 73%); ix) TFA/TIS/H_2O (y: 68%).

after 12 h, the obtainment of **12** in 78% isolated yield. It is worth mentioning that by replacing isobutyl chloroformate and NMM with 1-[bis(dimethylamino)methylene]−1H-1,2,3-triazolo[4,5-b]pyridinium 3-oxide hexafluorophosphate (HATU) and N, N-diisopropylethylamine (DIPEA), respectively, the condensation between **7a** and **11** was driven to completion in only 3 h and almost quantitative 98% yield. In the following step, the Cbz protecting group of compound **12** was removed through hydrogenolysis with $Pd(OH)_2$ catalyst (y: 87%), and L-aspartic acid-4 tert-butyl ester was coupled. The procedure involving isobutyl chloroformate as condensing agent afforded the desired product in 81% yield, whereas by using HATU compound **13** was obtained in 96% yield. Remarkably, the Cbz cleavage and the condensation with the Asp residue leading to **13** were also performed by avoiding purification of the N-deprotected intermediate in unaffected 83% overall yield.

Owing to the low efficiency of the Gly methyl ester hydrolysis under conventional basic conditions, an alternative approach was adopted. The linear pentapeptide was thus equipped for the final cyclization by converting the Gly methyl ester into the benzyl ester via $Ti(iPrO)_4$-catalyzed transesterification with benzyl alcohol.

Compound **14**, isolated in 84% yield, was then submitted to $Pd(OH)_2$ catalyzed hydrogenolysis to contemporary remove the Cbz protective group and the benzyl ester moiety from the amine and the carboxylic function, respectively, which were then intramolecularly condensed with HATU to give the cyclopentapeptide **15** in overall 73% yield. The last step involved the cleavage of the protective groups onto the side chains of **15**. Treatment with trifluoroacetic acid (TFA) in the presence of triisopropylsilane (TIS) as radical scavenger afforded, after 2.5 h, the fully deprotected cyclopentapeptide **16**. The crude mixture was diluted in water and directly submitted to preparative HPLC purification allowing the obtainment of the desired product, as TFA salt, in 73% yield.

2.2. Synthesis and characterization of cRGD-liposomes DOX

Firstly, the synthesis of the liposomes was performed in parallel by comparing two different methods: thin-film hydration method vs microfluidic strategy.

For thin-film hydration, a lipid mixture comprising 1,2-dimyristoyl-sn-glycero-3-phosphocholine (DMPC), 1,2-distearoyl-sn-glycero-3-phosphoethanolamine-N-[dibenzocyclooctyl(polyethylene glycol)-2000] (ammonium salt) (DBCO), DTPA-bis(stearylamide) (gadolinium salt), and 1,2-dioleoyl-sn-glycero-3-phosphoethanolamine-N-(lissamine rhodamine B sulfonyl) (ammonium salt) in 84:10:5:1 proportion was dissolved in chloroform. The subsequent removal of the solvent was achieved through rotatory evaporation and dry nitrogen stream, resulting in the formation of a lipid film on the flask walls. Rehydration and sonication of the lipid film with distilled water led to the generation of liposomes.

On the other hand, to promote the microfluidic-assisted synthesis of liposomes, different parameters were studied to assess how they impact on the liposomes characteristics: different total flow rates (TFRs) of 0.5, 1 and 1.5 ml/ min were studied at both 25 and 37 °C. In this case, to dissolve the lipid mixture, to facilitate diffusion into the aqueous phase and promote liposome self-assembly, ethanol was employed as the polar solvent.

The liposomes produced using the microfluidic strategy demonstrated that a TFR ranging from 0.5 to 1.5 ml/min at a temperature of 25 °C had a minimal impact on liposome size. In contrast, at 37 °C, TFR variation significantly influenced the size of the liposomes, with smaller liposomes being produced at a TFR of 0.5 ml/min. The PDI exhibited notable variations with TFRs variation. More specifically, at both temperatures, PDI values were higher at a TFR of 0.5 ml/min, decreasing below 0.3 at TFRs of 1 and 1.5 ml/min (see Supporting Information, Fig. S1).

The empty liposomes synthesized by the thin-film hydration method exhibit sizes comparable to those produced using the microfluidic technique at a TFR of 1 ml/ min at 25 °C. However, the required synthetic time by microfluidic technique is much lesser. Consequently, for subsequent experiments, liposomes synthesized *via* the microfluidic method were used due to the ease of synthesis and the achievement of similar size characteristics. Furthermore, the microfluidic technique offers significant advantages, being faster, easily scalable, and highly reproducible.

After optimizing the microfluidic-assisted synthesis of bare liposomes, doxorubicin salt encapsulation was promoted employing a remote loading strategy based on the creation of a buffer gradients across the liposome membrane. First, liposomes were resuspended in

diammonium phosphate buffer. Then, the extra-liposomal solution was substituted with HEPES buffered saline (HBS). After buffer exchanges, liposomes were incubated with a doxorubicin hydrochloride salt solution (DOX) in diammonium phosphate buffer at a drug-to-lipid molar ratio of 1:3. After 2 h, liposomes DOX were purified and washed with HBS to obtain the final liposomes DOX. The whole loading process in a liposome endowed with both a fluorescent tag and gadolinium as MRI contrast agent is summarized in Fig. 1.

Following the buffer exchange and a 2-hour incubation of the liposomes with DOX at 65 °C, drug encapsulation was assessed through HPLC analysis. Obtained results indicate that employing this remote loading method a DOX encapsulation yield exceeding 65% ± 5.38 % can be achieved corresponding to approximately 0.15 mg DOX per mg of lipid. These values were obtained from five independent liposome synthesis ($n = 5$).

The final step of the liposome's preparation involved their decoration with the cRGD derivatives. To this aim we focused our attention on a Strain-Promoted Azide-Alkyne Cycloaddition (SPAAC) reaction (Mbua et al., 2011). To perform this copper free click chemistry transformation, following the incorporation of a dibenzocyclooctine-modified (DBCO) lipid in the liposomes' membrane, the introduction of a complementary azide group on the cRGD directing moiety was mandatory. Therefore, the 5-azido pentanoic N-hydroxysuccinimide (NHS) ester **17** (Scheme 4) was synthetized according to the published procedure (Seo et al., 2003) and reacted with **16** to gain the modified derivative **N_3-cRGD**. This apparently easy condensation reaction required careful experimentation. The optimized reaction conditions, i.e. 25 °C, the use of DMF as a solvent, and triethylamine to maintain pH at 8.0, afforded after 24 h the azido-functionalized cyclopentapeptide **N_3-cRGD** in 62% yield. The TFA salt of **N_3-cRGD** arising from HPLC purification was then engaged in a SPAAC reaction with the DBCO-modified liposomes in $NaHCO_3$ buffer giving, after 20 h, the corresponding cRGD-decorated liposomes (Scheme 4).

The final functionalization rate was measured using HPLC yielding an average cRGD-surface modification value of 50% approximately.

The hydrodynamic size and polydispersity index (PDI) of liposomes was measured after each modification step (doxorubicin loading and cRGD surface modification) by DLS techniques (Supporting Information, Table S1). The size of the liposomes slightly increased upon remote loading with DOX, with the hydrodynamic size increasing from 112.5 nm for bare liposomes up to 124.8 nm for liposomes DOX. Conversely, when the drug-loaded liposomes were modified with the cRGD peptide, the size remained relatively stable at around 120 nm. Nevertheless, the Polydispersity Index (PDI) was consistently below 0.3 in all three cases, indicating the monodisperse nature of final cRGD-liposomes DOX.

To predict the colloidal stability in physiological environment, the surface ζ-potential profile of the three synthesized liposomes was assessed by DLS within the 2–11 pH range. The retrieved values did not show significant differences (Supporting Information, Fig. S2). In fact, all liposomes exhibited a negative ζ-potential of about −10 mV within the entire pH range, thus, ensuring colloidal stability in physiological environment.

The final cRGD-liposomes DOX were also characterized by Transmission Electron Microscopy (TEM) in order to study liposome morphology and size (Fig. 2). After liposomes staining with phosphotungstic acid (PTA), the images were acquired retrieving spherical shaped liposomes with an average size of approximately 60 (±17) nm.

The physicochemical properties of the liposomes, including particle size, polydispersity index (PDI), and encapsulation efficiency (EE%), were analyzed by the techniques previously detailed and the results remained consistent over a week period (data not shown). All parameters exhibited variations below 10%, indicating good colloidal and chemical stability of the formulation under storage conditions.

2.3. MRI and fluorescence imaging phantoms

Gadolinium (Gd) is commonly used as a contrast agent in MRI to enhance the visibility of certain tissues. The contrast of gadolinium in MRI arises from its ability to affect the relaxation times of nearby water protons in tissues. More specifically, gadolinium primarily affects the T_1 relaxation time, leading to increased signal intensity in T_1-weighted MRI images. T_1-weighted images are often used to highlight anatomical details and provide better contrast between different tissues. Nevertheless, the contrast enhancement depends on various factors, including the concentration of the gadolinium contrast agent. For that reason, to analyse the diagnostic capability of the synthesized liposomes, MRI studies were performed. With this purpose, several dilutions from final liposome suspension at known Gd concentrations (5, 10, 50, 100 and 150 μg/mL) were prepared and phantom images (Fig. 3A) were acquired using a 1 Tesla benchtop MRI scanner.

To complementary confirm the potential application of synthesized liposomes as contrast agents in MRI, longitudinal (R1) and transverse (R2) relaxation rates at 1.5 T were measured by using a benchtop relaxometer.

A transversal r_2 value of 18.84 $mM^{-1}s^{-1}$ and a longitudinal r_1 value of 6.66 $mM^{-1}s^{-1}$ r_1 were observed, with a final r_2/r_1 ratio lower than 3 (2,83) (Supporting Information, Table S2). In general, this ratio value is used to indicate the expected behavior of the molecular contrast agent to

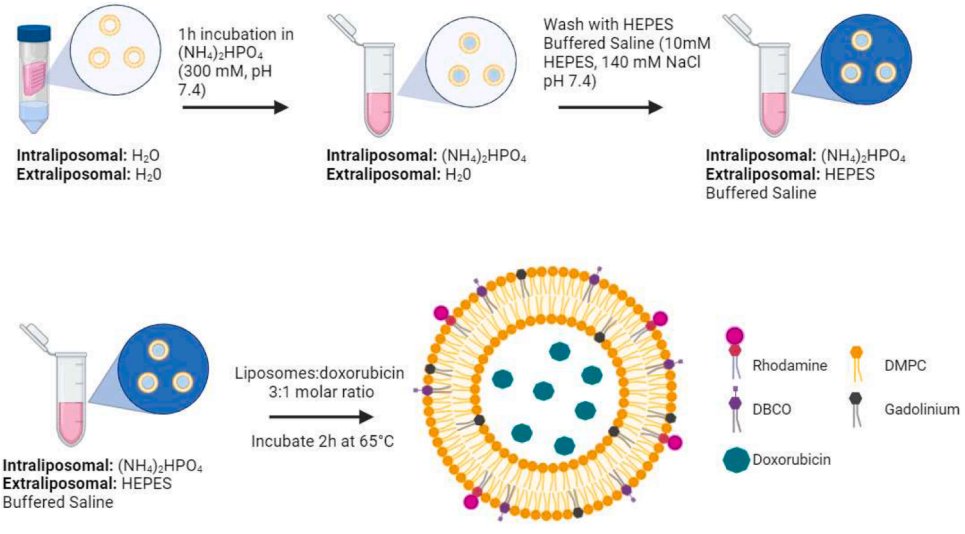

Fig. 1. Intra/extra liposomal buffer exchange procedure and remote loading of Doxorubicin hydrochloride salt into the liposomes.

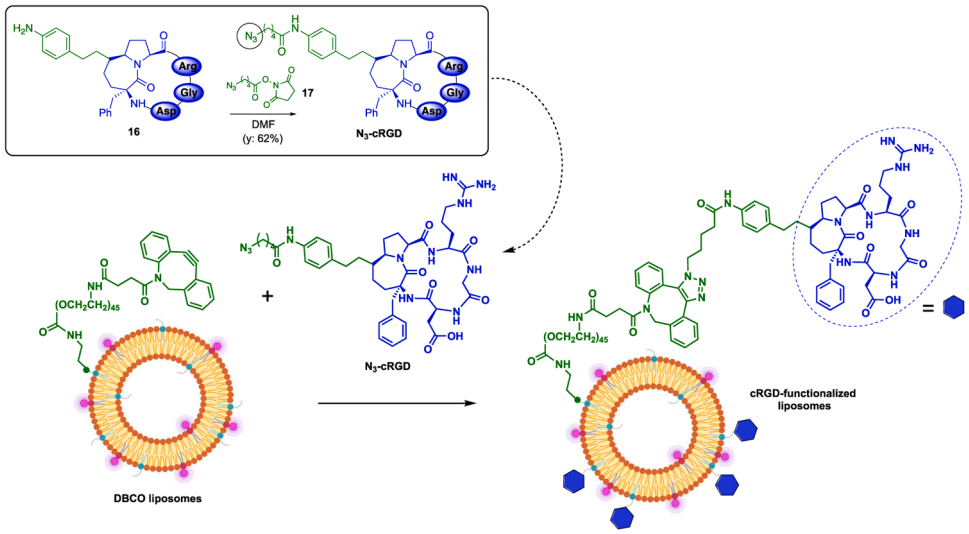

Scheme 4. Synthesis of N_3-cRGD and its use for liposome's functionalization.

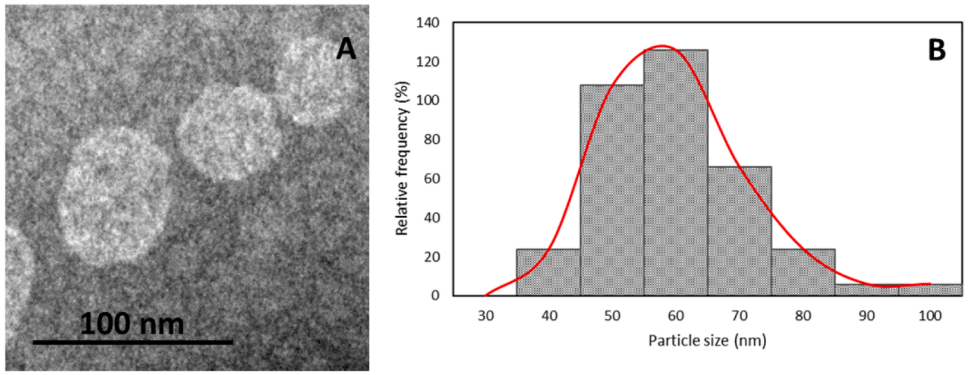

Fig. 2. TEM micrograph of synthesized liposomes (**A**) and mean size distribution ($n = 100$) (**B**).

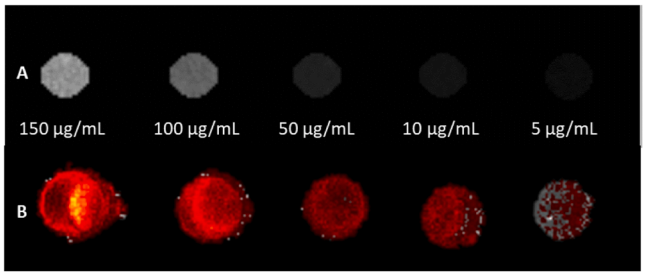

Fig. 3. Phantom images of the prepared liposomes at different Gd concentrations by MRI (A) and fluorescence imaging (B) techniques.

promote T_1-positive or T_2-negative MRI imaging, and in our case, it is in agreement with the phantoms' results that showed a very strong trend in promoting T_1-weighted MRI imaging (Fig. 3A). In fact, the lower the ratio, the higher the T_1 behaviour (Marciello et al., 2016; Zahraei et al., 2016; Luengo Morato et al., 2021; Lazaro-Carrillo et al., 2020; Sánchez et al., 2018). Furthermore, the results achieved with our theranostic nanoparticles are extremely promising especially in comparison to other commercially available contrast agents that are largely used in clinical settings. For example, the Combidex (Guerbet), Resovist (Schering), and Endorem (Ferropharm) magnetic nanoparticles showed r_2/r_1 ratios of 7, 9, and 12, respectively.

Additionally, due to the incorporation of the fluorescent lipid Liss Rhod PE (560/583 nm ex/em), fluorescent images at different Gd-lipid concentrations were obtained using the *in vivo* Imaging System (IVIS) 200 series (Fig. 3B). A linear enhancement of fluorescence signal as a function of concentration was appreciated, thus, confirming the usefulness of these multifunctional liposomes to promote the dual molecular imaging modality by optical and magnetic resonance techniques.

2.4. Assessment of integrin overexpression on the cancer cells surface

Before assessing the enhanced internalization of liposomes in cancer cells facilitated by the presence of the cRGD peptide, the overexpression of $\alpha_v\beta_3$ integrins in the selected cell lines (A375, human malignant melanoma; MG63, human osteosarcoma; PANC-1, human pancreatic carcinoma; and MDA-MB-231, triple-negative breast cancer) was investigated using immunostaining assays. These cell lines were chosen based on a literature review suggesting that they either overexpress or do not express $\alpha_v\beta_3$. To validate this, a specific primary antibody targeting the mentioned integrins was used, along with a suitable secondary antibody conjugated with a fluorescent dye. As reported in Fig. 4, the overexpression of $\alpha_v\beta_3$ integrin can be clearly and undoubtedly appreciated by Confocal Laser Scanning Microscopy (CLSM) only on the surface of MDA-MB-231 cells. Conversely, the target integrins did not show signs of overexpression on the surface of the other cancer cell lines (A375, MG63 and PANC-1).

2.5. Cellular uptake

Following their synthesis and characterization, the targeting

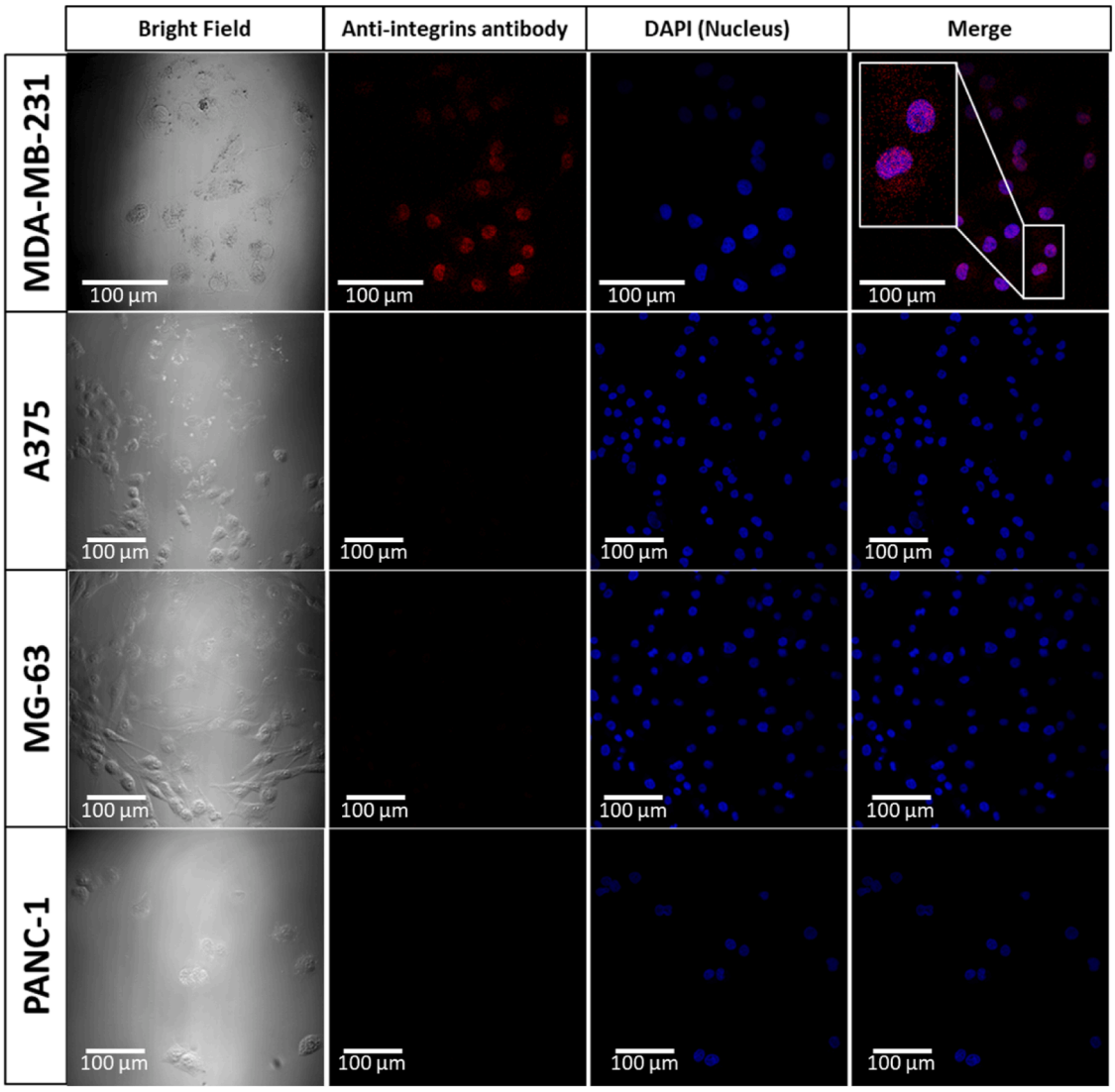

Fig. 4. $\alpha_v\beta_3$ integrin expression in MDA-MB-231, A375, MG-63 and PANC-1 cell lines. In blue the cellular nucleus stained with DAPI, in red the antibodies anti-$\alpha_V\beta_3$.

efficiency and enhanced uptake capabilities of cRGD-liposomes DOX were studied. Due to the confirmed overexpression of $\alpha_v\beta_3$ integrin receptors, TNBC cell line MDA-MB-231 was selected for the next studies. MDA-MB-231 cells were seeded and incubated overnight with equivalent amounts of fluorescent cRGD-functionalized and non-functionalized liposomes DOX. After incubation and washing, the cells were analyzed by CLSM. Representative images (Fig. 5) demonstrate that, following overnight incubation, the overall rhodamine fluorescence (in pink) is significantly higher in cells treated with cRGD-functionalized liposomes. These findings suggest that liposome uptake was integrin-mediated, resulting in greater intracellular accumulation when cells were exposed to cRGD-functionalized liposomes.

To further demonstrate that cellular uptake was mediated by $\alpha_v\beta_3$ integrin receptors and specifically promoted by cRGD functionalization on the liposome surface, an additional uptake experiment was performed. In this case, MDA-MB-231 cells were pre-incubated with free cRGD peptide to occupy the integrin receptors and to competitively inhibit integrin-mediated internalization of the targeted liposomal formulations. Thus, after the blocking pre-incubation, MDA-MB-231 cells were then exposed overnight to cRGD-functionalized DOX-loaded liposomes. After that, samples were washed and analysed using confocal laser scanning microscopy (CLSM). Representative images shown in Fig. 6 reveal a markedly lesser uptake in cancer cells that were pre-treated with free cRGD, thus, confirming that liposome internalization is integrin-mediated.

Besides the canonical 2D *in vitro* assessment, the cellular uptake of cRGD-targeted liposomes was also evaluated in MDA-MB-231 spheroids to assess their behavior in a 3D tumor-like structure. After their synthesis, spheroids were incubated for 4 h with either cRGD-functionalized or non-functionalized liposomes and analyzed by CLSM microscopy. As shown in Fig. 7A, the tumor cells within the 3D structure exhibited greater uptake of cRGD-functionalized liposomes. In this experimental series, fluorescence comparison following volumetric reconstruction revealed that fluorescence intensity within the spheroid, particularly at the periphery, was approximately 1.4 times higher in samples treated with cRGD-functionalized liposomes (Fig. 7B).

These results are consistent with those obtained in the 2D *in vitro* evaluation and confirm that cRGD-targeted liposomes show an enhanced ability to penetrate MDA-MB-231 cells, even in their more realistic 3D tumour-like spatial configuration.

2.6. *Antitumoral properties assessment*

After assessing the enhancing effect of cell targeting and internalization, the consequent expected DOX activity enhancement within cancer cells was studied. To this scope, the MTT toxicity assay was

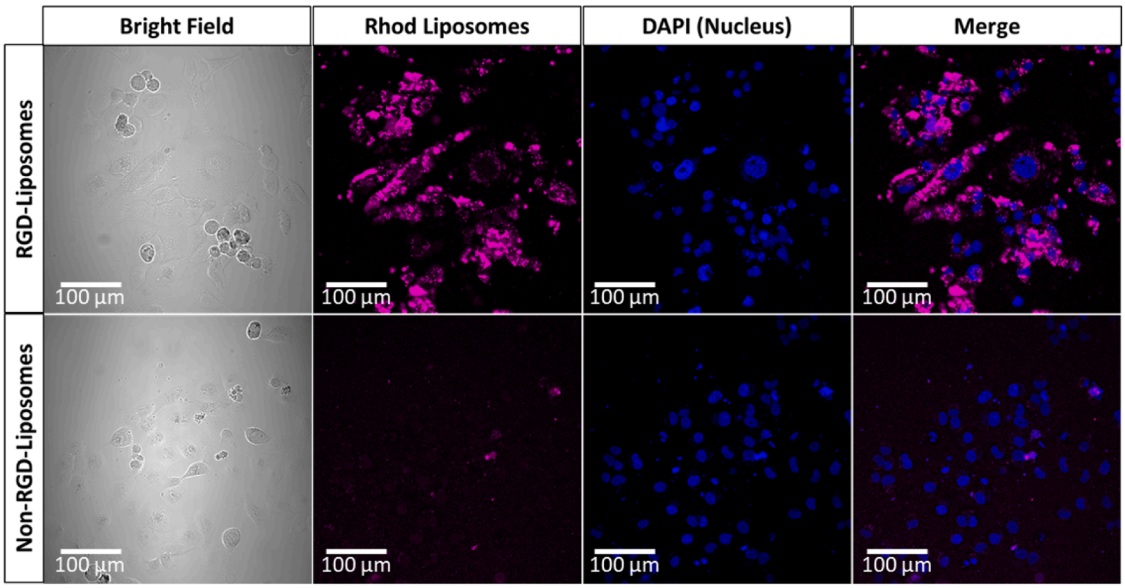

Fig. 5. Functionalized and non-functionalized liposomes internalization in MDA-MB-231 cell line, followed by confocal microscopy. In blue the cellular nucleus stained with DAPI, in pink the synthesized fluorescent liposomes.

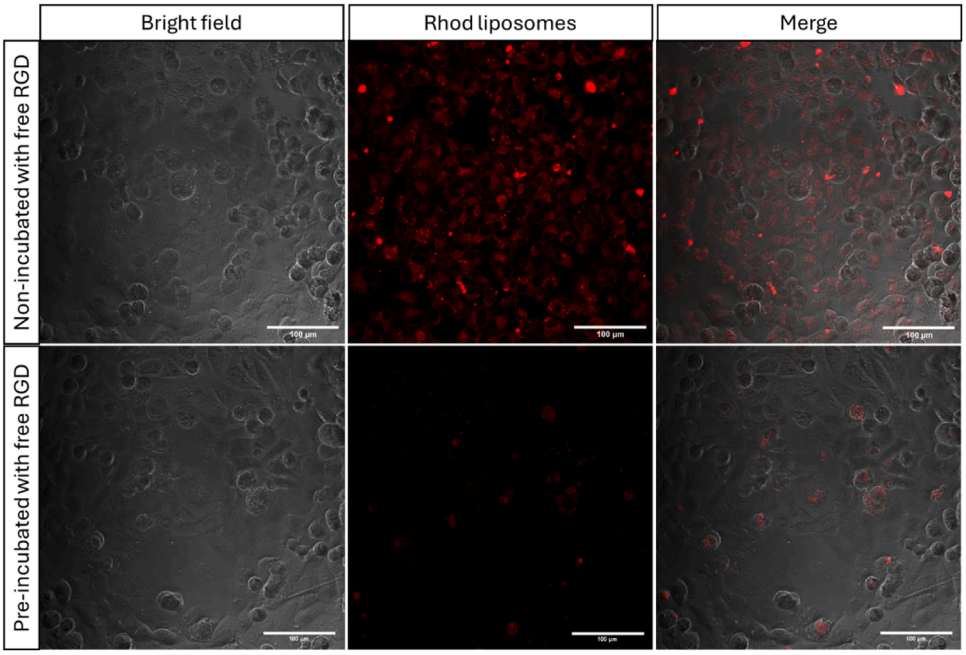

Fig. 6. **c**RGD-functionalized liposomes internalization in cRGD-preincubated and no preincubated MDA-MB-231 cells, followed by confocal microscopy. In red the synthesized fluorescent liposomes.

carried out after 48 h of incubation with either free DOX, liposomes DOX, or cRGD-liposomes DOX (Fig. 8) and obtained IC_{50} values were calculated (Table 1). As shown in Fig. 8A and Table 1, $a > 20$-fold enhancement of toxicity of targeted cRGD-liposomes DOX can be seen when compared to untargeted liposomes DOX on MDA-MB-231 cells. However, free DOX does not seem more toxic to the MDA-MB-231 cell line than liposomes DOX. Nevertheless, Fig. 8B–D suggest an opposite effect when testing the A375, PANC-1, and MG-63 cell lines. In fact, because of the absence of integrin overexpression on their cell surface, in all cases, targeted cRGD-liposomes DOX did not show an enhanced cellular toxicity compared to the untargeted liposomes DOX (Table 1). Furthermore, in the case of MG63 and PANC-1, free DOX is significantly more toxic to the cells than both liposomes DOX and cRGD-liposomes DOX in all three cell lines.

After confirming their enhanced antiproliferative properties with 2D *in vitro* cell viability assay, the behavior of the cRGD-targeted liposomes was also tested in a more realistic *in vitro* cell model as in the case of 3D tumour-like spheroids of MDA-MB-231 cells. In fact, as in the previous case, the 3D distribution of cancer cells embedded in a collagen matrix is expected to hamper the passive diffusion of the free drug as well as of the not targeted liposomes. Thus, as demonstrated previously, the decoration of the liposomes' outer surface with our cRGD peptide is expected to enhance the penetration of the nanodrug and, therefore, the antitumoral activity.

As shown in Fig. 9, the same concentration range as for the 2D *in vitro* model was studied. In all cases, the free drug was not effective at all and

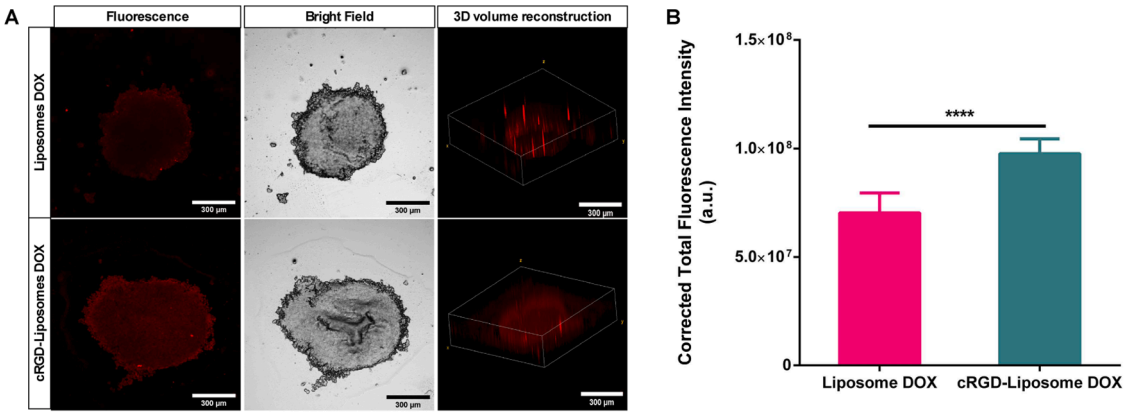

Fig. 7. **(A)** CLSM images of 3D spheroids of MDA-MB-231 cells incubated with cRGD-liposomes and not targeted liposomes. Color legend: cRGD-functionalized liposomes are in red (Rhodamine, Ex.560 /Em.583 nm). B) Total fluorescence comparison between reconstructed 3D spheroids incubated with not targeted liposomes and cRGD-targeted liposomes ($n = 10$ for each data series). Significance was calculated with an unpaired t-test with Welch's correction; ****: $p < 0.0001$.

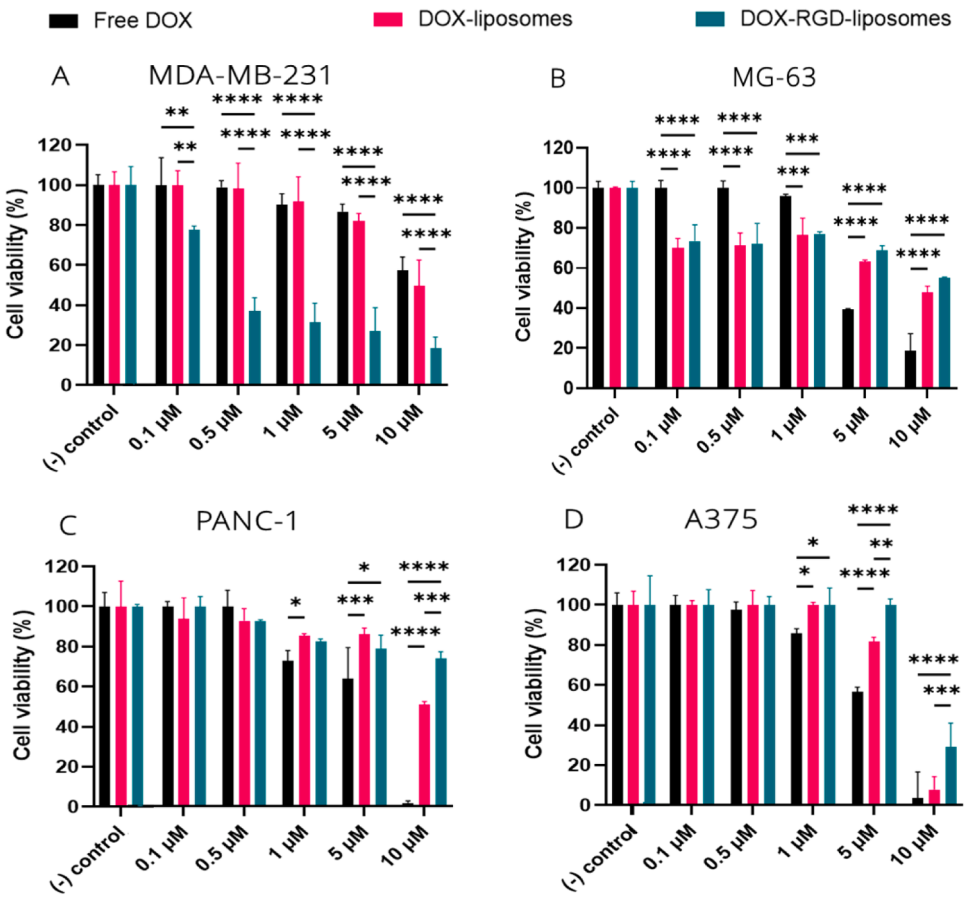

Fig. 8. Cell viability assays in 2D models: free doxorubicin (DOX), liposomes DOX and cRGD-liposomes DOX when incubated for 48 h in MDA-MB-231 (A), MG-63 (B), PANC-1 (C) and A375 (D) cell lines. $n = 3$ wells per condition. A 2-way ANOVA with multiple comparisons study was performed to analyse all data from the MTT toxicity assay ($\alpha = 0.05$, *$p < 0.1234$, **$p < 0.0332$, ***$p < 0.0021$, ****$p < 0.0001$).

the spheroid viability was kept constant. When liposomes were added, a decrease in cell viability was observed as a function of the increasing DOX concentration and depending on the presence or absence of the cRGD peptide. In fact, at all concentrations, the cRGD-targeted liposomes exhibited greater reduction in cell viability, confirming their superior ability to diffuse within the more complex 3D cell structures and promote enhanced antiproliferative activity (Fig. 9). These results support the enhanced cRGD-mediated penetration of our targeted liposomes and demonstrate the suitability of using spheroids for a more realistic *in vitro* evaluation of this novel nanodrug under development.

2.7. Cell migration inhibition

Besides the evaluation of the antitumor activity, we also investigated the ability of the liposomal formulations to inhibit MDA-MB-231 cell migration using a wound healing assay (Fig. 10), an *in vitro* method to assess collective cell migration in two dimensions that is also known as sheet migration. This migration behavior typically occurs in processes

Table 1
IC_{50} values of synthesized liposomes DOX.

Cell line	Free DOX (μM)	Liposome DOX (μM)	cRGD-liposomes DOX (μM)	Toxicity increase
MDA-MB-231	>10	>10	0.51	> 20x
MG63	4.25	9.3	>10	~1x
PANC-1	6.13	>10	>10	~1x
A375	5.29	1.70	1.43	~1x

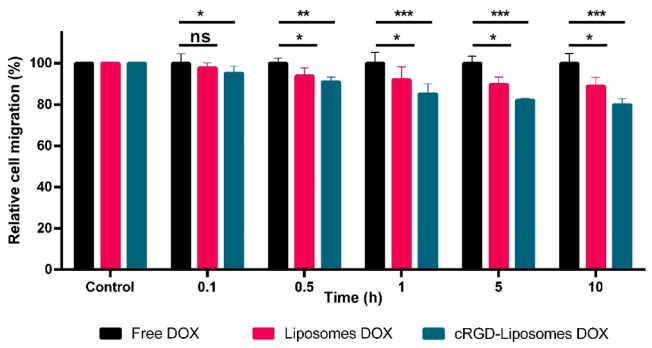

Fig. 9. Cell viability assays in 3D models: free doxorubicin (DOX), liposomes DOX and cRGD-liposomes DOX when incubated for 24 h in MDA-MB-231 cells. $n = 7$ wells per condition. Significance was calculated by one-way ANOVA Tukey's test. ns: $p > 0.05$ or not significant statistical difference between the groups of data; *: $p < 0.05$ or significant statistical difference between the groups of data; **: $p < 0.01$ or significant statistical difference between the groups of data; ***: $p < 0.001$ or significant statistical difference between the groups of data.

such as cancer metastasis (Lecomte et al., 2011; Hai et al., 2012; Fujisawa et al., 2012) To focus on migration effects while minimizing cytotoxicity, the assay was performed using DOX concentrations of 0.1 μM, corresponding to a sub-IC_{50} dose as previously determined by MTT assay (Table 1). The results indicate a clear inhibition of MDA-MB-231 cell migration in response to liposomal treatment in general (Fig. 10) and especially upon incubation with the cRGD-targeted ones. The percentage of inhibition was calculated by comparing during the time the remaining wound area with the initial gap area after treatment.

3. Conclusions

The results presented in this work describe the reproducible large-scale preparation of multifunctional liposomes with a cyclic RGD-based $\alpha_v\beta_3$ integrin inhibitor as advanced theranostic agent with high selectivity and efficacy against TNBC. We have detailed the complete synthetic pathway leading to the desired cRGD derivative, including the chemical modification of the Aba scaffold, an optimized solution-phase method for attaching the RGD sequence, and the late-stage introduction of an azido-terminating arm onto the unprotected cRGD, enabling subsequent bioconjugation reactions.

The azide moiety of **N_3-cRGD** has been engaged in a SPAAC reaction with liposomes loaded with doxorubicin and carrying on their surface dibenzocyclooctine groups to afford cRGD-liposomes DOX, exhibiting a spherical shape and uniform distribution.

For the preparation of liposomes, we compared the conventional thin-film hydration method with the more innovative microfluidic technique. The microfluidic approach demonstrated clear advantages, being notably faster, more reproducible, scalable, and efficient.

Surface ζ-potential measurements indicated that the liposomes were negatively charged at all tested pH values, suggesting good colloidal stability at physiological pH, which is a crucial factor for enhancing the pharmacodynamics of liposomes *in vivo*. The encapsulation of doxorubicin in the liposomes has been successfully achieved by optimizing a remote loading process and achieving a good encapsulation efficiency of 65%, as previously described.

Molecular imaging capabilities were also assessed, showing that the synthesized cRGD-liposomes can be useful to promote both *T1*-weighted magnetic resonance imaging (MRI) and fluorescence imaging modalities. These diagnostic characteristics may result very important for *in vitro* and *in vivo* applications because they could allow the correct tracking and follow up of the nanoparticles, and, consequently, a direct visualization of the tumoral mass. In this context, the presence of a fluorescent dye enabled the optical tracking of liposome uptake by cells, allowing us to study how this uptake correlates with the overexpression of integrin receptors on the surface of various cancer cell lines.

In vitro toxicity studies carried out on 2D models revealed that cRGD-liposomes DOX exhibited increased cytotoxicity in MDA-MB-231 cells compared to untargeted liposomes DOX. However, no active targeting effects were observed in other cancer cell lines (PANC-1, A375, and MG-63). These findings underscore the critical role of integrin overexpression in the therapeutic efficacy of our cRGD-decorated liposomes. Cell lines lacking $\alpha_v\beta_3$ integrin receptor showed no significant differences in viability when treated with targeted versus untargeted liposomes DOX. Conversely, due to the increased internalization rate resulting from the overexpression of $\alpha_v\beta_3$ integrin receptor on the surface of MDA-MB-231 cells, as well as the presence of the cRGD targeting moiety on the liposomes' surface, the cRGD-liposomes DOX exhibited enhanced cellular toxicity ($IC_{50} > 20x$) compared to the untargeted liposomes DOX and free DOX when used to treat this aggressive cancer cell line. These results were further confirmed using 3D *in vitro* models, such as spheroids derived from the MDA-MB-231 cell line. In addition to their enhanced antitumour activity, cRGD-targeted liposomes were shown to have potential antimigratory effects. Owing to the presence of the targeting peptide on their outer surface, the liposomes were able to inhibit the migration of MDA-MB-231 cells even at a very low doxorubicin concentration.

However, despite the very promising results achieved, we acknowledge that several translational challenges must be addressed before moving forward to clinical application. One key issue is the potential uptake by the reticuloendothelial system (RES), particularly in the liver and spleen, which could represent a significant barrier to effective tumor delivery. Although PEGylation was employed to extend circulation time and reduce opsonization, further optimization, such as tuning PEG density and length and lipid composition, will be required to minimize RES clearance. Secondly, off-target biodistribution could occur due to the presence of $\alpha_v\beta_3$ integrins in non-tumoral tissues, including some endothelial and immune cell populations. Nevertheless, the combination of passive targeting through the enhanced permeability and retention (EPR) effect and careful control of cRGD surface density may help increase tumor specificity. Finally, potential immunogenicity must be considered. While PEGylation can mitigate immune detection, repeated dosing may induce the "accelerated blood clearance" (ABC) phenomenon. Additionally, although the free RGD peptide has been generally demonstrated as non-immunogenic, its potential immune responses cannot be entirely ruled out depending on its nanoformulated form and on the administration route and dosing schedule. These factors will need to be thoroughly investigated in dedicated preclinical safety studies.

Taken together, these findings lay a solid foundation for the further *in vivo* evaluation of these potentially advanced theranostic nanoplatforms in orthotopic xenograft mouse models of triple-negative breast cancer, with a view to developing a powerful next-generation theranostic tool that could support the progress of precision medicine.

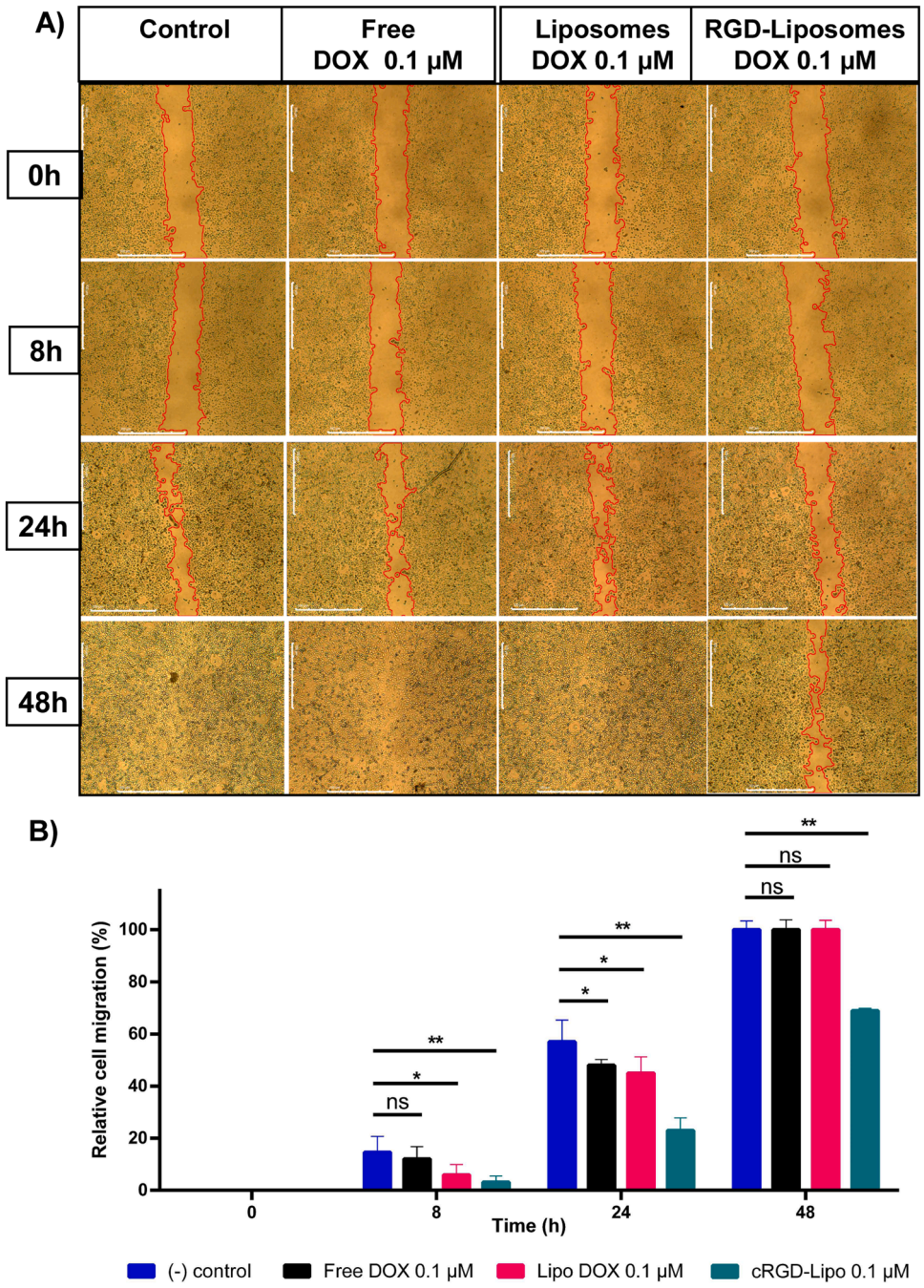

Fig. 10. Wound healing assay of MDA-MB-231 cells. (A) Phase contrast microscopy images of wells. The edges of the scar are marked in red. Control: cells grown in culture media (complete migration and wound healing). (B) Quantification of cell migration. The results were expressed as % of the initial scar area ($n = 3$ independent experiments). Significance was calculated by one-way ANOVA Tukey's test. ns: $p > 0.05$ or not significant statistical difference between the groups of data; *: $p < 0.01$ or significant statistical difference between the groups of data; **: $p < 0.01$ or significant statistical difference between the groups of data.

4. Experimental section

4.1. Synthesis

Synthesis of methyl (3S,9aR)-6-((((9H-fluoren-9-yl)methoxy) carbonyl)amino)-6-benzyl-9-((E)-4-((tert-butoxycarbonyl)amino) styryl)-5-oxo-2,3,5,6,7,9a-hexahydro-1H-pyrrolo[1,2-a]azepine-3-carboxylate (3)

Compound 1 (300 mg, 0.533 mmol) and styrene derivative 2 (234 mg, 1.07 mmol) were solubilized in toluene (0.017 M) and the solution was heated to 80 °C. Hoveyda-Grubbs II generation catalyst (33.4 mg, 10% mol) was dissolved in toluene (0.002 M) and slowly added to the reaction mixture over 7 h using a syringe pump. After 1 h from the end of the addition the solvent was evaporated under reduced pressure. The crude mixture was purified by flash chromatography to obtain 3 as a mixture of diastereoisomers.

Diastereoisomer 3a: White amorphous solid (96 mg, 24%). $R_f = 0.43$ (hexane/AcOEt 60:40); $[\alpha]_D^{22}$ +98.88 ($c = 1.0$, $CDCl_3$); ^{1}H NMR ($CDCl_3$, 400 MHz) δ 1.55 (s, 9H), 2.04–2.24 (m, 3H), 2.57–2.70 (m, 1H), 2.86 (d, $J = 17.6$ Hz, 1H), 3.42 (d, $J = 14.1$ Hz, 1H), 3.54 (dd, $J = 8.1$, 17.6 Hz, 1H), 3.70 (d, $J = 14.1$ Hz, 1H), 3.76 (s, 3H), 4.18–4.29 (m, 2H), 4.46–4.57 (m, 1H), 4.76 (d, $J = 6.7$ Hz, 1H), 4.88 (br s, 1H), 6.10 (br d, $J = 7.5$ Hz, 1H), 6.56 (d, $J = 16.0$ Hz, 1H), 6.61 (d, $J = 16.0$ Hz, 1H), 6.69 (s, 1H), 7.06 (br s, 2H), 7.15–7.26 (m, 3H), 7.29–7.46 (m, 9H), 7.53 (d, J

= 7.2 Hz, 1H), 7.62 (d, J = 7.3 Hz, 1H), 7.79 (d, J = 7.5 Hz, 2H); $^{13}C\{^1H\}$ NMR ($CDCl_3$, 100 MHz) δ 26.8 (t), 28.8 (3C), 33.9 (2C, t), 36.1 (t), 47.6, 52.8, 62.4, 62.8, 63.0 (s), 66.8 (t), 81.1 (s), 119.0 (2C), 120.3 (2C), 124.6, 125.6, 125.8, 127.3, 127.4 (3C), 127.5, 128.0 (2C), 128.1, 128.8 (2C), 129.5, 129.7 (2C), 132.1 (s), 136.9 (s), 137.3 (s), 138.5 (s), 141.6 (s), 141.7 (s), 144.3 (s), 144.5 (s), 153.1 (s), 154.7 (s), 172.3 (s), 172.7 (s); IR (neat, cm^{-1}) 3368, 3029, 2979, 2932, 2848, 1716, 1630, 1587, 1519, 1491, 1411, 1314, 1222, 1154, 1070, 1051; HRMS (ESI) calculated for $C_{46}H_{47}N_3O_7Na$ $[M+Na]^+$ 776.33062 found 776.33105 (Δ = 0.6 ppm)

Diastereoisomer 3b: White amorphous solid (120 mg, 30%). R_f = 0.15 (AcOEt/hexane 60:40); $[\alpha]_D^{22}$ +22.40 (c = 1.0, $CDCl_3$); ^1H NMR ($CDCl_3$, 400 MHz) δ 1.54 (s, 9H), 1.94–2.09 (m, 3H), 2.32–2.41 (m, 1H), 2.46 (dd, J = 8.3, 18.4 Hz, 1H), 2.68 (d, J = 18.4 Hz, 1H), 3.05 (d, J = 14.2 Hz, 1H), 3.62 (d, J = 14.2 Hz, 1H), 3.75 (s, 3H), 4.23 (t, J = 5.9 Hz, 1H), 4.38 (br s, 1H), 4.64 (d, J = 5.9 Hz, 2H), 4.78– 4.91 (m, 2H), 5.66 (br d, J = 6.9 Hz, 1H), 6.37 (d, J = 16.0 Hz, 1H), 6.43 (d, J = 16.0 Hz, 1H), 6.57 (br s, 1H), 6.99–7.06 (m, 2H), 7.22–7.28 (m, 5H), 7.29–7.38 (m, 5H), 7.38–7.46 (m, 2H), 7.62 (t, J = 6.5 Hz, 2H), 7.77 (t, J = 6.9 Hz, 1H), 7); $^{13}C\{^1H\}$ NMR ($CDCl_3$, 100 MHz) δ 26.7 (t), 28.8 (3C), 33.5 (2C, t), 40.3 (t), 47.9, 52.6, 59.8 (s), 59.9, 62.1, 66.3 (t), 81.2 (s), 118.9 (2C), 120.4, 120.5, 121.2, 125.2, 125.3, 127.0, 127.4 (2C), 127.5, 127.5, 127.9, 128.1, 128.2, 128.6 (2C), 129.5, 131.8 (2C), 132.3 (s), 136.9 (s), 138.3 (s), 138.5 (s), 140.5 (s), 141.8 (s), 141.9 (s), 144.1 (s), 153.0 (s), 155.1 (s), 171.7 (s), 173.3 (s); IR (neat, cm^{-1}) 3323, 3026, 2963, 2927, 2854, 1721, 1638, 1589, 1520, 1496, 1411, 1315, 1262, 1156, 1103, 1028. HRMS (ESI) calculated for $C_{46}H_{47}N_3O_7Na$ $[M+Na]^+$ 776.33062 found 776.33137 (Δ = 1.0 ppm)

Synthesis of methyl (3S,6R,9S,9aR)-6-((((9H-fluoren-9-yl)methoxy) carbonyl)amino)-6-benzyl-9-(4-((tert-butoxycarbonyl)amino)phenethyl)-5-oxooctahydro-1H-pyrrolo[1,2-a]azepine-3-carboxylate (4a)

To a solution of 3a (365 mg, 0.484 mmol) in dry MeOH (9.7 mL, 0.05 M), under H_2 (balloon), PtO_2 (platinum oxide) was added (4 mg, 1 % weight). The reaction mixture was stirred at room temperature for 24 h. Formation of the product was monitored by TLC analysis, R_f = 0.48 (hexane/AcOEt 60:40). The reaction mixture was filtered through a pad of Celite, and the organic phase was evaporated under reduced pressure. The crude mixture was purified by flash chromatography (hexane/AcOEt 70:30) to obtain pure compound 4a as a white amorphous solid (334 mg, 91%). *Rf* = 0.31. $[\alpha]_D^{22}$ −10,80 (c = 1.0, $CDCl_3$); ^1H NMR (dmso-d_6, 80 °C, 400 MHz) δ 1.49 (s, 9H), 1.63–2.18 (m, 11H), 2.35–2.45 (m, 1H), 2.58–2.69 (m, 1H), 3.18 (br s, 1H), 3.33 (d, J = 12.5 Hz, 1H), 3.53 (s, 3H), 4.11 (dd, J = 3.8, 8.6 Hz, 1H), 4.27 (t, J = 5.9 Hz, 1H), 4.31–4.46 (m, 2H), 4.54 (dd, J = 5.8, 10.5 Hz, 1H), 6.26 (br s, 1H), 6.82 (br s, 2H), 7.10 (d, J = 8.4 Hz, 2H), 7.13–7.19 (m, 3H), 7.31–7.38 (m, 4H), 7.39–7.45 (m, 2H), 7.65 (t, J = 8.2 Hz, 2H), 7.87 (d, J = 8.2 Hz, 2H), 8.89 (s, 1H); $^{13}C\{^1H\}$ NMR (dmso-d_6, 80 °C, 100 MHz) δ 26.7 (t), 27.0 (t), 27.6 (t), 27.7 (t), 29.1, 30.5 (t), 33.2 (t), 36.5 (t), 38.6, 47.9, 52.2, 62.6, 63.7, 64.7 (s), 66.2 (t), 79.7 (s), 119.5 (2C), 120.8 (2C), 125.6, 125.7, 127.3, 127.8 (2C), 127.9 (2C), 128.4 (2C), 128.7 (2C), 129.1 (2C), 130.3 (2C), 136.7 (s), 137.0 (s), 138.1 (s), 141.8 (s, 2C), 144.8 (s), 144.9 (s), 153.8 (s), 154.4 (s), 171.6 (s), 172.5 (s); IR (neat, cm^{-1}) 3364, 3029, 2978, 2932, 2877, 1719, 1626, 1594, 1521, 1486, 1448, 1412, 1366, 1313, 1225, 1155, 1077, 1050. HRMS (ESI) calculated for $C_{46}H_{51}N_3O_7Na$ $[M+Na]^+$ 780.36192 found 780.36267 (Δ = 1.0 ppm)

Synthesis of methyl (3S,6R,9S,9aR)-6-amino-6-benzyl-9-(4-((tert-butoxycarbonyl)amino) phenethyl)-5-oxooctahydro-1H-pyrrolo [1,2-a]azepine-3-carboxylate (5a)

To a solution of compound 4a (275 mg, 0.363 mmol) in dry THF (4.1 mL, 0.090 M) under nitrogen atmosphere, piperidine (36 μL, 0.36 mmol) was added. Formation of the product was monitored by TLC, R_f = 0.34 (AcOEt/MeOH 95:05). After 6 h the solvent was evaporated under reduced pressure and the crude mixture was purified by flash chromatography (AcOEt/MeOH 95:05) to obtain compound 5a as a white amorphous solid (167 mg, 85%). R_f = 0.34.

Synthesis of (3S,6R,9S,9aR)-6-benzyl-6-(((benzyloxy)carbonyl) amino)-9-(4-((tert-butoxycarbonyl) amino)phenethyl)-5-oxooctahydro-1H-pyrrolo[1,2-a]azepine-3-carboxylic acid (7a)

Compound 5a (71 mg, 0.13 mmol) was dissolved in dry THF (1.3 mL, 0.10 M) under nitrogen atmosphere and cooled to 0 °C. The reaction mixture was added with Cbz_2O (49 mg, 0.17 mmol) and, after 2 h, was warmed to room temperature. After 16 h the reaction mixture was added with a 1.6 M aqueous solution of LiOH (166 μL, 0.265 mmol). If needed, MeOH can be added to homogenize the solution and, afterwards, the reaction mixture was heated to 60 °C. After 16 h the solvent was evaporated under reduced pressure, the residue was recovered with water, the pH was adjusted to 2 by addition of a 0.01 M HCl aqueous solution and the aqueous layer was extracted three times with AcOEt. The organic phase was dried with anhydrous Na_2SO_4, filtered, and the solvent was evaporated under reduced pressure. The crude mixture was purified by flash chromatography (AcOEt/MeOH 99:01) to obtain compound 7a as a white amorphous solid (82 mg, 96%). R_f = 0.45. $[\alpha]_D^{22}$ −82,94 (c = 1.0, $CDCl_3$); ^1H NMR ($CDCl_3$, 400 MHz) δ 1.54 (s, 9H), 1.56–1.67 (m, 2H), 1.69–1.80 (m, 1H), 1.81–2.14 (m, 6H), 2.32–2.47 (m, 2H), 2.66–2.76 (m, 1H), 2.89 (br s, 1H), 3.38 (d, J = 13.9 Hz, 1H), 3.61 (d, J = 13.9 Hz, 1H), 4.29 (br s, 1H), 4.43 (d, J = 7.2 Hz, 1H), 5.08 (d, J = 12.4 Hz, 1H), 5.24 (d, J = 12.4 Hz, 1H), 6.56 (br s, 2H), 6.86 (d, J = 6.9 Hz, 2H), 7.07 (d, J = 8.4 Hz, 2H), 7.14–7.30 (m, 5H), 7.32–7.45 (m, 5H), 10.85 (br s, 1H); $^{13}C\{^1H\}$ NMR ($CDCl_3$, 100 MHz) δ 26.1 (t), 26.7 (t), 26.8 (t), 28.8 (3C), 30.1 (t), 30.3 (t), 32.3 (t), 32.4 (t), 36.5, 64.4, 65.3 (s), 66.6 (t), 81.0 (s), 119.4 (2C), 127.6, 128.5, 128.8 (2C), 128.9 (2C), 129.1 (2C), 129.7 (2C), 136.1 (s), 136.2 (s), 136.8 (s), 137.2 (s), 153.5 (s), 154.6 (s), 172.0 (s), 174.9 (s); IR (neat, cm^{-1}) 3600–2600 (broad band), 3354, 2961, 2929, 2856, 1716, 1624, 1593, 1520, 1485, 1447, 1412, 1366, 1313, 1227, 1156, 1075, 1049, 1026. HRMS (ESI) calculated for $C_{38}H_{45}N_3O_7Na$ $[M+Na]^+$ 678.31497 found 678.31520 (Δ = 0.3 ppm).

Synthesis of methyl N^2-(((9*H*-fluoren-9-yl)methoxy)carbonyl)-N^{ω}-((2,2,4,6,7-pentamethyl-2,3-dihydrobenzofuran-5-yl)sulfonyl)- l-arginylglycinate (10).

To a solution of Fmoc-Arg(Pbf-OH) (250 mg, 0.385 mmol, 1eq) and N-Methylmorpholine (84μl, 0.770 mmol, 2eq) in dry THF [0.1 M], cooled to 0 °C, isobutyl chloroformate (60μl, 0.462 mmol, 1.2eq) was added. After 20 min H_2N-Gly-OMe*HCl (58 mg, 0.462 mmol, 1.2eq) 9 was added, and the reaction mixture was allowed to warm to room temperature and stirred for 2 h. Then, the solvent was removed and the mixture, resolubilized in EtOAc, was washed once with 1 M HCl and once with saturated $NaHCO_3$. The organic phase was dried over Na_2SO_4, filtered, and evaporated under reduced pressure. The crude was purified by flash column chromatography (DCM/acetone 75:25) to afford 10 as a white amorphous solid (207 mg, 75%). The reaction was monitored by TLC analysis (DCM /Acetone 70:30, R_f = 0.5).

^1H NMR ($CDCl_3$, 400 MHz) δ 1.45 (s, 6H), 1.58–1.69 (m,2H), 1.77 (m, 1H), 1.97 (m, 1H), 2.09 (s, 3H), 2.53 (s, 3H), 2.60 (s, 3H), 2.93 (s, 2H), 3.25 (m, 1H9, 3.36 (m, 1H), 3.70 (s, 3H), 3.92 (dd, J = 5.5, 17.9 Hz, 1H), 4.09 (dd, J = 6.2, 18.0 Hz, 1H), 4.16 (t, J = 7.0 Hz, 1H), 4.30–4.46 (m, 3H), 6.09 (br S, 2H), 6.34 (br S, 2H), 7.26 (t, J = 7.5 Hz, 2H), 7.38 (t, J = 7.5 Hz, 2H), 7.53–7.61 (m, 2H), 7.67 (br S, 1H), 7.75 (d, J = 7.5 Hz, 2H); $^{13}C\{^1H\}$ NMR ($CDCl_3$, 100 MHz) δ 12.5, 17.9, 19.3, 25.1 (t), 28.6, 30.2 (t), 40.2 (t), 41.1 (t), 43.2 (t), 47.1, 52.3, 54.0, 67.1 (t), 86.4 (s), 117.6 (s), 199.9, 124.7 (s), 125.1, 127.1, 127.7, 132.3 (s), 132.5 (s), 128.4 (s), 141.2 (s), 143.7 (s), 143.8 (s), 156.5 (s), 158.9 (s), 170.8 (s), 172.8 (s); IR (neat, cm^{-1}) 3436, 3314, 2927, 1715, 1663, 1616, 1548, 1448, 1239, 1209, 1089, 1032. HRMS (ESI) calculated for $C_{37}H_{46}N_5O_8S$ $[M + H]^+$ 720.3062, found 720.3057 (Δ = –0.6 ppm).

Synthesis of methyl N^{ω} -((2,2,4,6,7-pentamethyl-2,3-dihydrobenzofuran-5-yl)sulfonyl)- l-arginylglycinate (11)

To a solution of dipeptide 10 (100 mg, 0.138 mmol, 1eq) in THF [0.1 M] piperidine (21 ml, 0.213 mmol, 1.5eq) was added and the mixture stirred at rt for 2 h.

The solvent was evaporated under reduced pressure, and the crude

resuspended in HCl 0.5 M and washed 2 times with EtOAc. The inorganic phase was then basified with Na_2CO_3 solution and extracted 3 times with EtOAc. The reunified organic phases were dried over Na_2SO_4 anhydrous, filtered and concentrated in vacuo. The obtained amorphous white solid was triturated with hexane and used without further purification (56 mg, y: 82%).

The reaction was monitored by TLC analysis (DCM/Acetone 70:30) to determine depletion of the starting material (product $R_f = 0.4$, DCM/MeOH 80:20).

Synthesis of methyl N^2-((3S,6R,9S,9aR)-6-benzyl-6-(((benzyloxy) carbonyl)amino)-9-(4-((tert-butoxycarbonyl)amino)phenethyl)-5-oxo octahydro-1H-pyrrolo[1,2-a]azepine-3-carbonyl)-N^{ω}-((2,2,4,6,7-pentamethyl-2,3-dihydrobenzofuran-5-yl)sulfonyl)-l-arginylglycinate (12)

Compound 7a (85 mg, 0.13 mmol) and compound 11 (128 mg, 0.259 mmol) were dissolved in dry THF (1.3 mL, 0.10 M). The reaction mixture was added with HATU (98 mg, 0.26 mmol) and DIPEA (47 μL, 0.26 mmol) and was left stirring for 3 h. Afterwards, the solvent was evaporated under reduced pressure, the residue was recovered with CH_2Cl_2 and was washed with a 1 M $KHSO_4$ aqueous solution and a saturated $NaHCO_3$ aqueous solution. The organic phase was dried with anhydrous Na_2SO_4, filtered, and the solvent was evaporated under reduced pressure. The crude mixture was purified by flash chromatography (AcOEt/hexane 90:10) to obtain compound 12 as a white amorphous solid (148 mg, 98%). $R_f = 0.34$. $[\alpha]_D^{22}$ −28,86 ($c = 1.0$, $CDCl_3$); ^{1}H NMR ($CDCl_3$, 400 MHz) δ 1.46 (s, 6H), 1.54 (s, 9H), 1.55–2.15 (m, 11H), 2.09 (s, 3H), 2.23 (br s, 1H), 2.31–2.43 (m, 2H), 2.49–2.66 (m, 2H), 2.53 (s, 3H), 2.61 (s, 3H), 2.86–2.94 (m, 1H), 2.95 (s, 2H), 3.26 (br s, 1H), 3.38 (d, $J = 13.8$ Hz, 1H), 3.56 (d, $J = 13.8$ Hz, 1H), 3.68 (s, 3H), 3.90 (dd, $J = 5.6$, 17.6 Hz, 1H), 4.01 (dd, $J = 5.6$, 17.6 Hz, 1H), 4.35 (br s, 2H), 4.53 (d, $J = 6.9$ Hz, 1H), 5.03 (d, $J = 12.3$ Hz, 1H), 5.24 (d, $J = 12.3$ Hz, 1H), 5.95 (br s, 1H), 6.15 (br s, 2H), 6.68 (br s, 1H), 6.77 (br s, 1H), 6.84 (d, $J = 6.7$ Hz, 2H), 7.08 (d, $J = 7.9$ Hz, 2H), 7.12–7.25 (m, 5H), 7.32–7.45 (m, 5H), 7.48 (br s, 1H), 7.82 (br s, 1H); ^{13}C{^{1}H} NMR ($CDCl_3$, 100 MHz) δ 12.9, 18.3, 19.7, 25.9 (br t), 26.3 (br t), 26.9 (t), 27.7 (2C, br t), 28.8 (3C), 29.0 (2C), 29.9 (t), 30.1 (t), 30.8 (t), 33.5 (t), 38.1, 39.0, 39.7 (br t), 41.4 (t), 43.6 (t), 52.6, 63.4 (br), 64.3, 65.1 (s), 66.6 (t), 81.0 (s), 86.9 (s), 118.0 (s), 120.9, 125.1 (s), 127.5, 128.4 (2C), 128.6 (2C), 128.8 (2C), 128.9 (2C), 129.4 (2C), 129.9 (2C), 132.9 (s), 135.9 (s), 136.3 (s), 137.1 (s), 137.8 (s), 138.9 (s), 154.4 (s), 155.1 (s), 156.5 (s), 159.3 (s), 166.2 (s), 170.9 (s), 171.2 (s), 172.7 (s), 173.4 (s); IR (neat, cm^{-1}) 3600–2600 (broad band), 3329, 2963, 2928, 2855, 1720, 1664, 1613, 1522, 1449, 1411, 1367, 1313, 1304, 1261, 1234, 1157, 1090, 1049, 1026. HRMS (ESI) calculated for $C_{60}H_{76}N_6O_{12}SNa$ $[M+Na]^+$ 1157.53521 found 1157.53449 (Δ = 0.6 ppm)

Synthesis of tert-butyl (*S*)-4-(((3S,6R,9S,9aR)-6-benzyl-9-(4-((tert-butoxycarbonyl) amino) phenethyl)-3-(((*S*)-1-((2-methoxy-2-oxoethyl) amino)-1-oxo-5-(3-((2,2,4,6,7-pentamethyl-2,3-dihydrobenzofuran-5-yl)sulfonyl)guanidino)pentan-2-yl)carbamoyl)-5-oxooctahydro-1H-pyrrolo[1,2-a]azepin-6-yl)amino)-3-(((benzyloxy)carbonyl)amino)-4-oxobutanoate (13)

To a solution of compound 12 (130 mg, 0.115 mmol) in dry MeOH (1.2 mL, 0.10 M), under H_2 (balloon), $Pd(OH)_2$/C (13 mg, 10% weight) was added. The reaction mixture was stirred at room temperature for 24 h. Afterwards, it was filtered through a pad of Celite and the organic phase was evaporated under reduced pressure. The crude mixture was dissolved in dry THF (1.2 mL, 0.10 M) under nitrogen atmosphere and was added with Z-L-Asp(O*t*Bu)-OH (74 mg, 0.23 mmol), HATU (98 mg, 0.26 mmol) and DIPEA (47 μL, 0.26 mmol). After 3 h, the solvent was evaporated under reduced pressure, the residue was recovered with CH_2Cl_2 and was washed with a 1 M $KHSO_4$ aqueous solution and a saturated $NaHCO_3$ aqueous solution. The organic phase was dried with anhydrous Na_2SO_4, filtered, and the solvent was evaporated under reduced pressure. The crude mixture was purified by flash chromatography (AcOEt/hexane 80:20) to give compound 13 as a white amorphous solid (125 mg, 83%). $R_f = 0.35$. $[\alpha]_D^{22}$ −42,84 ($c = 1.0$, $CDCl_3$); ^{1}H NMR (dmso-d_6, 400 MHz) δ 1.29–1.43 (m, 3H), 1.38 (s, 9H), 1.40 (s, 6H), 1.47 (s, 9H), 1.50–1.61 (m, 2H), 1.64–1.76 (m, 2H), 1.78–2.06 (m, 7H), 1.98 (s, 3H), 2.27–2.38 (m, 1H), 2.40 (s, 3H), 2.42–2.45 (m, 1H), 2.46 (s, 3H), 2.54–2.63 (m, 1H), 2.69 (dd, $J = 5.5$, 15.8 Hz, 1H), 2.79 (br s, 1H), 2.86–3.03 (m, 4H), 3.41 (d, $J = 13.6$ Hz, 1H), 3.51 (d, $J = 13.6$ Hz, 1H), 3.60 (s, 3H), 3.74–3.89 (m, 2H), 4.10–4.19 (m, 1H), 4.20–4.27 (m, 1H), 4.32–4.43 (m, 2H), 4.97 (d, $J = 12.6$ Hz, 1H), 5.05 (d, $J = 12.6$ Hz, 1H), 6.39 (br s, 1H), 6.63 (br s, 1H), 6.92 (d, $J = 6.1$ Hz, 2H), 7.04 (d, $J = 8.4$ Hz, 2H), 7.10–7.22 (m, 3H), 7.22–7.38 (m, 7H), 7.77 (d, $J = 8.4$ Hz, 1H), 7.84–7.92 (m, 2H), 8.23 (t, $J = 5.6$ Hz, 1H), 9.18 (s, 1H); ^{13}C{^{1}H} NMR ($CDCl_3$, 100 MHz) δ 12.3, 17.9, 19.3, 25.0 (br t), 26.1 (t), 27.1 (br t), 27.3 (br t), 27.9 (3C), 28.3 (3C), 28.5 (2C), 29.2 (t), 29.5 (t), 29.6 (t), 32.3 (t), 36.5 (t), 38.7, 51.2, 52.2, 52.9, 60.0 (br), 64.0, 65.3 (s), 67.1 (t), 80.2 (s), 81.5 (s), 86.6 (s), 117.7 (s), 119.4 (2C), 124.9 (s), 127.5, 127.9 (2C), 128.2, 128.5 (6C), 130.0 (2C), 133.3 (s), 134.7 (s), 136.0 (s), 136.2 (s), 136.4 (s), 139.3 (s), 153.3 (s), 155.2 (s), 156.8 (s), 159.5 (s), 169.9 (s), 170.2 (s), 171.0 (s), 171.7 (s), 173.0 (s), 173.5 (s); IR (neat, cm^{-1}) 3600–2600 (broad band), 3336, 2977, 2928, 2869, 1723, 1665, 1616, 1525, 1453, 1411, 1367, 1294, 1235, 1158, 1108, 1088, 1051. HRMS (ESI) calculated for $C_{68}H_{91}N_9O_{15}SNa$ $[M+Na]^+$ 1328.62475 found 1328.62317 (Δ = −0.7 ppm)

Synthesis of tert-butyl (*S*)-4-(((3S,6R,9S,9aR)-6-benzyl-3-(((*S*)-1-((2-(benzyloxy)-2-oxoethyl) amino)-1-oxo-5-(3-((2,2,4,6,7-pentamethyl-2,3-dihydrobenzofuran-5-yl) sulfonyl)guanidino) pentan-2-yl)carbamoyl)-9-(4-((tert-butoxycarbonyl)amino) phenethyl)-5-oxooctahydro-1H-pyrrolo[1,2-a]azepin-6-yl)amino)-3-(((benzyloxy) carbonyl)amino)-4-oxobutanoate (14)

To a solution of compound 13 (281 mg, 0.216 mmol) in dry THF (2.2 mL, 0.10 M), under nitrogen atmosphere, BnOH (2.2 mL, 21.56 mmol), Ti(*i*PrO)$_4$ (32 μL, 0.108 mmol) and 4 Å molecular sieves (450 mg) were added. The reaction mixture was heated to 90 °C and was left stirring for 16 h. Afterwards, the mixture was filtered through a pad of Celite and the organic phase was evaporated under reduced pressure. The residue was recovered with CH_2Cl_2 and was washed two times with a 2 M HCl aqueous solution. The organic phase was dried with anhydrous Na_2SO_4, filtered, and the solvent was evaporated under reduced pressure. The crude mixture was purified by flash chromatography (CH_2Cl_2/MeOH 95:05) to give compound 14 as a white amorphous solid (250 mg, 84%). $R_f = 0.38$. $[\alpha]_D^{22}$ −42,20 ($c = 1.0$, $CDCl_3$); ^{1}H NMR (dmso-d_6, 60 °C, 400 MHz) δ 1.31–1.44 (m, 3H), 1.39 (s, 9H), 1.40 (s, 6H), 1.48 (s, 9H), 1.53–1.64 (m, 2H), 1.68–2.03 (m, 9H), 2.00 (s, 3H), 2.30–2.39 (m, 1H), 2.43 (s, 3H), 2.44–2.49 (m, 1H), 2.48 (s, 3H), 2.53–2.62 (m, 1H), 2.70 (dd, $J = 5.5$, 15.8 Hz, 1H), 2.74–2.81 (m, 1H), 2.89–3.01 (m, 4H), 3.41 (d, $J = 13.7$ Hz, 1H), 3.53 (d, $J = 13.7$ Hz, 1H), 3.81–3.95 (m, 2H), 4.14–4.22 (m, 1H), 4.23–4.29 (m, 1H), 4.30–4.42 (m, 2H), 4.99 (d, $J = 12.6$ Hz, 1H), 5.04 (d, $J = 12.6$ Hz, 1H), 5.11 (s, 2H), 6.42 (br s, 1H), 6.54 (br s, 1H), 6.95 (d, $J = 6.3$ Hz, 2H), 7.04 (d, $J = 8.4$ Hz, 2H), 7.13–7.22 (m, 3H), 7.24–7.39 (m, 12H), 7.54 (br s, 1H), 7.73 (d, $J = 8.1$ Hz, 1H), 7.81–7.89 (m, 1H), 8.10 (t, $J = 5.7$ Hz, 1H), 8.97 (s, 1H); ^{13}C{^{1}H} NMR (dmso-d_6, 60 °C, 100 MHz) δ 12.0, 17.4, 18.7, 25.2 (t), 26.1 (t), 26.2 (t), 26.8 (t), 27.8 (3C), 28.2 (5C), 28.6 (t), 28.9 (t), 29.3 (t), 29.6 (t), 32.3 (t), 34.5 (t), 37.0, 38.7, 37.6 (t), 40.8 (t), 42.7 (t), 52.3, 53.1, 61.8, 63.5, 64.9 (s), 65.7 (t), 65.9 (t), 78.8 (s), 80.1 (s), 86.1 (s), 116.2 (s), 118.6 (2C), 124.3 (s), 126.5, 127.4 (2C), 127.6, 127.8 (2C), 127.8 (2C), 127.9, 128.2 (2C), 128.2 (2C), 128.3 (2C), 129.6 (2C), 131.5 (s), 134.5 (s), 135.6 (s), 135.9 (s), 136.3 (s), 136.8 (s), 137.2 (s), 152.9 (s), 155.6 (s), 156.1 (s), 157.5 (s), 169.2 (s), 169.4 (s), 169.5 (s), 170.7 (s), 171.3 (s), 171.8 (s); IR (neat, cm^{-1}) 3600–2600 (broad band), 3327, 2970, 2927, 2869, 1722, 1663, 1615, 1523, 1454, 1411, 1367, 1236, 1156, 1108, 1089, 1051, 1028. HRMS (ESI) calculated for $C_{74}H_{95}N_9O_{15}SNa$ $[M+Na]^+$ 1404.65605 found 1404.65662 (Δ = 0.4 ppm)

Synthesis of compound 15

To a solution of compound 14 (134 mg, 0.0970 mmol) in dry MeOH (1.9 mL, 0.050 M), under H_2 (balloon), $Pd(OH)_2$/C (13 mg, 10% weight) was added. The reaction mixture was stirred at room temperature for 12 h. Afterwards, it was filtered through a pad of Celite and the organic

phase was evaporated under reduced pressure. The crude mixture was dissolved in dry THF (24 mL, 0.0040 M) under nitrogen atmosphere and was added with HATU (74 mg, 0.19 mmol) and DIPEA (35 μL, 0.19 mmol. After 24 h, the solvent was evaporated under reduced pressure and the crude mixture was purified by flash chromatography (AcOEt/MeOH 98:02) to obtain compound 15 as a white amorphous solid (81 mg, 73%). R_f = 0.30. $[\alpha]_D^{22}$ −21.60 (c = 1.3, $CDCl_3$); IR (neat, cm^{-1}) 3600–2600 (broad band), 3327, 2925, 2854, 1722, 1657, 1622, 1520, 1453, 1411, 1368, 1296, 1236, 1155, 1107, 1090, 1052, 1028. HRMS (ESI) calculated for $C_{59}H_{81}N_9O_{12}SNa$ $[M+Na]^+$ 1162.56176 found 1162.56360 (Δ = 1.6 ppm)

Synthesis of compound 16

Compound 15 (106 mg, 0.0929 mmol) was dissolved in a 95:2.5:2.5 TFA/triisopropylsilane/water solution (9.3 mL, 0.010 M) and the reaction mixture was stirred at room temperature for 2.5 h. Afterwards, the solution was diluted with 40 mL of water and the crude mixture was purified by preparative HPLC (stationary phase: C18, mobile phase: isocratic elution for 2 min with 95 % of water + 0.1 % CF_3CO_2H, then increasing gradient to 60 % of acetonitrile over 16 min, l = 210, 254 nm) to obtain 16 (trifluoroacetate salt) as a white amorphous solid (61 mg, 68%). ^{1}H NMR (D_2O, 60 °C, 400 MHz) δ 1.68–1.79 (m, 3H), 1.81–2.32 (m, 9H), 2.42 (m, 1H), 2.52 (m, 1H), 2.62–2.78 (m, 2H), 2.91 (m, 1H), 3.11 (dd, J = 6.7, 17.1 Hz, 1H), 3.17 (m, 1H), 3.25 (dd, J = 6.8, 17.0 Hz, 1H), 3.30–3.45 (m, 2H), 3.52 (d, J = 13.4 Hz, 1H), 3.80 (d, J = 13.4 Hz, 1H), 3.88 (d, J = 14.7 Hz, 1H), 4.29 (d, J = 14.6 Hz, 1H), 4.41 (dd, J = 8.1, 10.1 Hz, 1H), 4.65 (dd, J = 4.7, 8.0 Hz, 1H), 5.16 (t, J = 6.5 Hz, 1H), 7.34–7.40 (m, 2H), 7.56–7.77 (m, 7H); $^{13}C\{^1H\}$ NMR (D_2O, 100 MHz) δ 23.8 (t), 24.1 (t), 25.1 (t), 27.7 (t), 28.9 (t), 29.5 (t), 29.6 (t), 32.1 (t), 33.7 (t), 39.1, 40.2 (t), 40.4 (t), 44.0 (t), 50.1, 50.3, 51.7, 51.8, 65.6, 122.9, 127.4, 127.6 (s), 128.5, 130.0, 130.1, 135.4 (s), 143.6 (s), 156.7 (s), 170.5 (s), 171.9 (s), 173.8 (s), 174.0 (s), 174.7 (s), 174.8 (s); IR (neat, cm^{-1}) 3372, 2926, 2855, 1733, 1717, 1683, 1639, 1515, 1456, 1375, 1338, 1299, 1246, 1205, 1146, 1069; HRMS (ESI) calculated for $C_{37}H_{50}N_9O_7$ $[M + H]^+$ 732.38277 found 732.38379 (Δ = 1.4 ppm)

Synthesis of compound N_3-cRGD

Compound 16 (20.7 mg, 0.02156 mmol) was dissolved in DMF (0.4 mL, 0.05 M), under nitrogen atmosphere, and the pH was adjusted to 8.0 with Et_3N (0.03 mL, 0.2156 mmol). The NHS-activated linker 17 (15.5 mg, 0.065 mmol) was added at the reaction mixture at 0 °C, and after 10 min, the reaction was heated at 25 °C. After 24 h the solution was diluted with 32 mL of water + 0.1% CF_3COOH, and the crude product was purified by preparative HPLC (stationary phase: C18, mobile phase: isocratic elution for 2 min with 95% water + 0.1% CF_3COOH then increasing gradient to 60% of acetonitrile over 16 min, λ = 210 nm, 254 nm). The purified product was then freeze-dried to give the pure trifluoroacetate salt of the desired N_3-cRGD derivative as a white foam (13 mg, 0.01339 mmol, 62% yield). Spectroscopic data were in accordance with literature (Serra et al., 2023b).

4.2. Synthesis of liposomes

4.2.1. Thin-film hydration

A lipid mix comprising DMPC, DBCO, Gadolinium, and Rhodamine was dissolved in chloroform at a molar ratio of 84:10:5:1, respectively. Subsequently, the solvent was removed through evaporation using a rotatory evaporator (Büchi R-215, Buchegg, Switzerland) under the conditions of 120 millibar, 280 rpm, for 10 min at 40 °C, followed by a final step under a nitrogen flux to ensure complete lipid desiccation. The resulting lipid film was rehydrated and resuspended in filtered distilled water, subjected to sonication at 40 °C for 1 h, and then underwent purification and washing with filtered distilled water.

4.2.2. Microfluidic

To compare synthetic methods and improve the synthesis efficiency, liposomes were also prepared using the Dolomite (Royston, UK) microfluidic flow control device and software. Employing the same phospholipid composition (DMPC, DBCO, Gadolinium and Rhodamine) and ratio (84:10:5:1, respectively), different temperatures and flow rates were studied to investigate the impact of changing the synthesis conditions on the size and polydispersity of the liposomes. The phospholipids were dissolved in ethanol (≥99.8 % v/v) at a 2mg/ mL lipid concentration. The pre-prepared lipid phase was in one of the chambers, and the water was inserted to the second chamber. The lipid and aqueous phases were injected into a 5-input hydrophilic chip 3D with 150 μm channels diameter. Maintaining a constant flow rate ratio (FRR; 1:4, ethanol:water ratio) but changing the total flow rate (TFR; 0.5, 1 and 1.5 ml/min), different formulations were synthesized at 25 and 37 °C.

4.3. Doxorubicin encapsulation by remote loading strategy

The encapsulation of doxorubicin salt within plain liposomes was achieved through a remote loading strategy, involving the creation of distinct buffer gradients across the phospholipidic membrane (Fritze et al., 2006). To facilitate the ion gradient essential for drug encapsulation, intra and extraliposomal buffers underwent exchange. In brief, liposomes were re-suspended in diammonium phosphate buffer (300 mM $(NH_4)_2HPO_4$, pH 7.4) and incubated on a roller for 1 h at room temperature. Subsequently, the liposomes were subjected to purification with Amicon filters, washed with HEPES buffered saline (140 mM NaCl, 10 mM HEPES, pH 7.4) (HBS) to substitute the extra-liposomal solution, and filtered using a 0.22 μm 13 mm syringe filter (hydrophilic). The pH values of the utilized buffers were adjusted with 0.5 – 3.0 M HCl and 0.05 – 1.0 M NaOH.

Meanwhile, Doxorubicin HCl (DOX) was dissolved in diammonium phosphate buffer (300 mM, pH 7.4) to achieve a final concentration of 0.1 mg/ mL. The DOX solution was added to the liposomes at a drug-to-lipid molar ratio of 1:3 and incubated for 2 h at 65 °C in a shaker incubator operating at 300 rpm. Subsequently, the liposomes DOX underwent purification and washing with HBS.

To assess the yield of DOX encapsulation, while purifying and washing liposomes DOX with HBS, the supernatant obtained from the initial centrifugal cycle, conducted prior to liposome washing, was preserved. Following the completion of the washing process, liposomes DOX were recovered from the filters and re-suspended in HBS. To assess encapsulation efficiency, the supernatant from the liposomes and the 0.1 mg/ mL DOX solution initially administered to the liposomes were subjected to analysis using high-pressure liquid chromatography (HPLC), considering the dilution factor of the DOX solution during incubation with the liposomes. To quantify DOX encapsulated in the liposomes, the following HPLC method (Wei et al., 2008) was applied. In brief, the mobile phase consisted of a mixture of methanol-water (60:40) containing 0.1% formic acid (pH 3) and the analysis were carried out using a Gemini® 5 μm NX-C18 110 Å LC Column (250 × 4.6 mm, Phenomenex, Alcobendas, Spain) at 35 °C with a flow rate of 1 mL/min. All samples were analyzed at 480 nm, being approximately 5 min the retention time of the DOX. Previously, all samples were evaporated at 50 °C and rehydrated in the same volume with the mobile phase, then they were analyzed as described previously. The obtained chromatogram was used to determine encapsulation of DOX in the liposomes. Each prepared sample was quantified by extrapolation with a calibration curve (R^2: 0.997) prepared by using free DOX at known concentrations. Each sample was analyzed in triplicate.

Toward this scope, a comparison was made between the peak area of DOX in the liposome supernatant and the initial total amount of drug provided at the onset of the remote loading process. The encapsulation efficiency was quantified using formula (1):

$$Encapsulated\ DOX = \frac{DOX\ offered - DOX\ in\ supernatant}{DOX\ offered}\ x\ 100 \quad (1)$$

The HPLC equipment used was a LC-4000 HPLC system equipped with an interface box (LC—NetII/ADC), a photo diode-array detector

(MD-4010), a RHPLC pump (PU-4180) and a column oven (CO-4061) (JASCO, USA). The software used for the analysis and peak integration was ChromNAV, a software system from JASCO—HPLC analysis (Tokyo, Japan).

4.4. Surface modification of liposomes DOX by 'click' conjugation with the N_3–3a-RGD peptide

The cRGD peptide was linked to the surface of the liposomes by a SPAAC reaction. N_3-cRGD was dissolved in pure methanol and added to a sodium bicarbonate buffer (12 mM, pH 8.5) at a 5-times molar excess with respect to the DBCO lipid previously quantified as described below. Meanwhile, the liposomes DOX were purified in Amicon filters after which they were resuspended in the prepared cRGD-peptide solution and incubated for 2 h at room temperature on a roller incubator. Finally, the cRGD-liposomes DOX were purified and filtered using HBS.

To assess the yield of surface modification of the cRGD-peptide on the liposomes, the supernatant of the liposomes at the end of the SPAAC reaction as well as the initial cRGD-solution offered to the liposomes were analysed using HPLC. Briefly, the analyses were carried out using a Gemini® 5 μm NX-C18 110 Å LC Column (250 × 4.6 mm, Phenomenex, Alcobendas, Spain) with a flow rate of 1 mL/min and a gradient condition starting for the initial 2 min with 80% water + 0.1% CF_3COOH and 20% acetonitrile. Then, the gradient was increased to 80% acetonitrile during 6 min. Before the analysis, all samples were centrifuged and then measured as described above at 255 nm. The obtained chromatogram was used to determine cRGD surface modification rate of the liposomes by comparing cRGD representative peaks, being its retention time around 8 min. Each prepared sample was quantified by extrapolation with a calibration curve (R^2: 0.998) prepared by using free cRGD-peptide at known concentrations. Each sample was analyzed in triplicate.

The amount of cRGD-peptide immobilized over liposomes' surface was quantified by comparing the respective peak areas of the initial offered solution of N_3–3a-cRGD peptide vs the liposome supernatant recovered at the end of the reaction. The yield of liposomes DOX functionalization with cRGD-peptide was determined using the following formula (2).

$$cRGD\ surface\ functionalization = \left(\frac{cRGD\ offered - cRGD\ in\ supernatant}{Offered\ cRGD}\right) x\ 100 \quad (2)$$

The HPLC analyses were performed with a LC-4000 HPLC system equipped with an interface box (LC—NetII/ADC), a photo diode-array detector (MD-4010), a RHPLC pump (PU-4180) and a column oven (CO-4061) (JASCO, USA). The software used for the analysis and peak integration was ChromNAV, a software system from JASCO—HPLC analysis (Tokyo, Japan).

4.5. Physicochemical characterization

4.5.1. Hydrodynamic size and zeta-potential with dynamic light scattering (DLS)

Produced liposomes, including plain, liposomes DOX and cRGD-liposomes DOX, were analyzed in their hydrodynamic size distribution and surface z-potential using a Malvern Nano ZS-90 DLS instrument (ZEN3600, Worcestershire, UK) and analysed with Zetasizer Software (v7.04).

For zeta-potential measurements, liposomes DOX and cRGD-liposomes DOX were diluted in a solution of KNO_3 (0.01 M), with pH was adjustments carried out using KOH (0.05 M – 3 M) and HNO_3 (0.5 M). Zeta-potential was measured in triplicate at various pH values ranging from 2 to 11.

4.5.2. Lipid concentration

For the quantification of lipids in the synthesized liposomes, a Stewart assay was conducted (Stewart, 1980). Briefly, samples were evaporated overnight at 50 °C, followed by resuspension in chloroform and subsequent addition of ammonium ferrothiocyanate in a 1:1 (v/v) ratio. The resulting solutions were vortexed and centrifuged (1000 rpm, 10 min) leading to the separation of two phases. The chloroform layer was then analyzed in triplicate at a fixed wavelength of 488 nm using a JASCO V-730 spectrophotometer. The lipid concentration was determined by referencing the measurements against a previously established standard curve of these liposomes (R^2=0.994).

4.5.3. Transmission electron microscopy

The morphology and size of the synthesized liposomes were studied by transmission electron microscopy (TEM) on a JEM 1400 microscope (JEOL, Akishima, Tokyo, Japan). A blend of aqueous liposome suspensions and 2% phosphotungstic acid (PTA) at pH 5.4 in a 1:1 (v/v) ratio, was placed onto 200 mesh copper grids coated with formvar/carbon for 1 min. Then, the grids were allowed to air-dry, and images were acquired using the aforementioned microscope. The analysis of TEM images for size distribution was performed with ImageJ software.

4.5.4. Magnetic resonance and fluorescence imaging phantoms

The magnetic properties of the synthesized liposomes, attributed to the presence of Gd, were studied through magnetic resonance imaging (MRI) at BioImaC (ICTS BioImagen Complutense), a node of the ICTS ReDIB (https://www.redib.net/), using a 1 Tesla benchtop MRI scanner (ICON 1T-MRI; Bruker BioSpin GmbH, Ettlingen, Germany). The ICON 1T-MRI, featuring a permanent magnet and a gradient system with a capability of supplying 450 mT/m gradient strength, employed a linear polarized solenoid RF-coil (inner diameter 61 × 52 mm^2 and length 90 mm).

MRI data were collected using Paravision 6.0.1 software (Bruker, BioSpin). The primary MRI protocol involved a two-dimensional T_1-weighted experiment. Coronal anatomical sections were acquired using a spin echo sequence with a repetition time of 750 ms, and echo time of 7.5 ms, one average, a field of view of 35 × 11 mm^2, a slice thickness of 1.5 mm, and a total of 5 slices. The matrix size was 350 × 110 (resolution 0.200 × 0.200 × 1.50 mm), and the total acquisition time was approximately 1 min.

Additionally, due to the incorporation of the fluorescent lipid Liss Rhod PE (560/583 nm ex/em), fluorescent images at varying Gd-lipid concentrations were obtained using the IVIS Imaging System 200 series (Xenogen).

Both imaging techniques were performed to samples at different known Gd concentrations: 5, 10, 50, 100 and 150 μg/mL.

4.5.5. Relaxometry

To evaluate the efficiency of the synthesized liposomes as contrast agents, relaxation time measurements were also carried out in a MINISPEC MQ60 (Bruker) at 37 °C and a magnetic field of 1.5 T. The samples were prepared at different Gd concentrations and the relaxivity values (r_1 and r_2) were calculated by the liner fitting of the relaxation rates $R_{1,2}$ ($1/T_{1,2}$) values for each Gd concentration and blank solution.

4.6. In vitro studies

4.6.1. Cell lines and culture conditions

All cell lines were incubated at 37 °C and 5% CO_2. Cell lines A375 and MG63 were cultured in Dulbecco's Modified Eagle Medium (DMEM) with 10% fetal bovine serum (FBS) and 1% antibiotics (Penicillin/Streptomycin). PANC-1 cells were cultured in DMEM with 10% FBS, 1% Glutamine, and 1% antibiotics (Pen/Strep). Finally, MDA-MB-231 cells were cultured in DMEM – F12, containing 10% FBS, 1% non-essential aminoacids (NEAA), 1% sodium pyruvate, and 1% antibiotics (Pen/Strep).

3D spheroids of MDA-MB-231 were generated as described by Keller et al. (2019). Briefly, in a 96-well spheroid microplates (Corning), 30.000 MDA-MB-231 cells per well were seeded and 2.5% v/v of basement membrane extract (BME/Cultrex,) were added before centrifugating for 6 min at 500 rcf. The achieved spheroids were cultured 3 days in the specific medium previously described before their use.

4.6.2. Integrin expression evaluation

Total of 3×10^5 cells of A375, MDA-MB-231, PANC-1 and MG-63 cell lines were seeded in a 6-well culture plate. After 24 h, cells were fixed with 4% PFA pH 7.4 for 10 min at 37 °C and 5% CO_2. After washing 3 times with PBS 1X for 5 min each, a blocking solution of 5% Serum Goat in PBS 1X was added for 60 min at room temperature (RT). After the blocking solution, the incubation of the primary antibody was carried out. Briefly, the CD51/CD61 (Integrin alpha V beta 3) Monoclonal Antibody (23C6) (ThermoFisher Scientific) was incubated with the cells in 0.1% Serum Goat for 3 h at RT. Cells were washed 3 times with PBS 1X for 5 min each and incubated with the secondary antibody. In this case, the Alexa Fluor 647 Goat Anti Rabbit IgG ($H + L$) antibody (ThermoFisher Scientific, REF: A-21,245) was incubated with the cells in 0.1% Serum Goat for 45 min at RT. After that, cells were washed 3 times with PBS 1X for 5 min each. Cell nucleus was stained with DAPI (0.1% in media without phenol red) for 15 min. A control without the primary antibody was also studied to compare the specifical binding of the secondary antibody to the primary one. Images were obtained using a 20X objective in a confocal laser scanning microscope Zeiss LSM 780 (Ex/Em 647/670 nm for secondary antibody and 405/457 nm for DAPI) under 37 °C and 5% CO_2 conditions and they were processed with ImageJ software.

4.6.3. Cellular uptake

3×10^5 MDA-MB-231 cells were seeded in a 6-well culture plate. After 24 h of cellular growing, cells were incubated other 24 h with the functionalized and non-functionalized liposomes (with or without cRGD but both without DOX) in a 0.01 mg/ mL final lipid concentration. Then, cell nucleus was stained with DAPI (0.1% in media without phenol red) for 15 min. Images were obtained using a 20X objective in a confocal laser scanning microscope Zeiss LSM 780 (Ex/Em 560/583 nm for Rhodamine and 405/457 nm for DAPI) under 37 °C and 5% CO_2 conditions and they were processed with ImageJ software.

Additionally, another 6-well culture plate was seeded with 3×10^5 MDA-MB-231 cells per well and allowed to grow for 24 h. Cells were then pre-incubated for 1 h with free cRGD peptide at a final concentration of 0.25 mg/ mL. After this blocking step, the medium was replaced with fresh medium containing either functionalized or non-functionalized liposomes (with or without cRGD) at a final lipid concentration of 0.01 mg/ mL. Following a 4-hour incubation, images were acquired using a Zeiss LSM 780 confocal laser scanning microscope with a 20 × objective (Ex/Em 560/583 nm for Rhodamine), under standard culture conditions (37 °C, 5% CO_2). Image processing was performed using ImageJ software.

Finally, cellular uptake was also evaluated in 3D models. MDA-MB-231 spheroids were incubated for 4 h with either cRGD-functionalized or non-functionalized liposomes. Images were acquired using a Nikon A1-R confocal microscope equipped with a 10 × objective (Ex/Em 560/583 nm for Rhodamine), under standard culture conditions (37 °C, 5% CO_2). Image processing and fluorescence quantification were carried out using ImageJ software.

4.6.4. Cell viability

The MTT toxicity assay was carried out in the A375, MDA-MB-231, PANC-1 and MG-63 cell lines. DMEM without phenol red was used for the MTT assay to avoid interferences. Cells were seeded in a 96-wells plate to yield circa 80% confluency at the day of incubation with the liposomes. The cells were incubated for 24, 48, and 72 h (37 °C, 5% CO_2) with either liposomes DOX or cRGD-liposomes DOX at a DOX concentration ranging from 0.1 – 10 μM. After incubation with the liposomes, the supernatants were discarded, replaced with 100 μL of medium and 10 μL of MTT solution (5 mg/ mL) was added. After a 3-hour incubation (37 °C, 5% CO_2), the formazan salts generated were dissolved with DMSO and plates were analysed using the SPECTROstar Nano (BMG Labtech INC).

The same protocol was followed to perform the MTT cell viability assay in spheroids.

4.6.5. Cell migration

MDA-MB-231 cells (1.5×10^4 cells in 25 μL of medium) were seeded into each chamber of Allegro silicone inserts (Stencell™, Idylle Labs, Paris, France) placed in a 24-well plate. After 24 h of incubation to allow cell attachment and monolayer formation, the silicone inserts were carefully removed to create a defined cell-free gap. Cells were then treated with free DOX, liposomes DOX, or cRGD-liposomes DOX at concentrations of 0.1 μM for 24 h. Wound healing was monitored by imaging the same fields at 0, 8, 24, and 48 h using a Motic AE31E inverted trinocular microscope and comparing the remaining uncovered areas during the time.

4.7. Statistics and analysis

Statistical analysis was performed using Prism software (GraphPad), and all chart data were expressed as mean ± standard deviation (Mean ± SD).

Availability of data and materials

The datasets generated during and/or analysed during the current study are available from the corresponding authors on reasonable request.

CRediT authorship contribution statement

Karina Ovejero-Paredes: Investigation. **Giovanni Bisbano:** Investigation. **Inge Flier:** Investigation. **Alejandro González-Simón:** Investigation. **Marzia Marciello:** Supervision, Investigation. **Sabrina Oliveira:** Supervision, Investigation. **Marco Zupi:** Investigation. **Davide Rubes:** Investigation. **Fatima Ayash:** Investigation. **Filippo Doria:** Investigation. **Valentina Pirota:** Investigation. **Marco Terreni:** Supervision, Formal analysis. **Massimo Serra:** Writing – review & editing, Writing – original draft, Validation, Supervision, Methodology, Investigation, Data curation, Conceptualization. **Marco Filice:** Writing – review & editing, Writing – original draft, Validation, Supervision, Resources, Methodology, Investigation, Funding acquisition, Formal analysis, Data curation, Conceptualization.

Declaration of competing interest

The authors have no relevant financial or non-financial interests to disclose.

Acknowledgements

M.F. and M.M. are grateful to the European Commission for funding this research work (Project BRECISE; reference: 101194784). M.F. and M.M. are grateful to Instituto de Salud Carlos III (ISCIII) for project PI22/00789 (AES22-ISCIII) and PT23CIII/00006. K.O.P, M.F. and M.M. acknowledge the support of Microscopy & Dynamic Imaging Unit of CNIC, Madrid, Spain. The Unit is part of the ReDiB-ICTS and has the support of FEDER, "Una manera de hacer Europa." The CNIC is supported by the Instituto de Salud Carlos III (ISCIII), the Ministerio de Ciencia e Innovación (MCIN) and the Pro CNIC Foundation, and is a Severo Ochoa Center of Excellence (grant CEX2020-001041-S funded by MICIN/AEI/10.13039/501100011033).

Supplementary materials

Supplementary material associated with this article can be found, in the online version, at doi:10.1016/j.ejps.2025.107216.

Data availability

Data will be made available on request.

References

Alipour, M., Baneshi, M., Hosseinkhani, S., Mahmoudi, R., Arabzadeh, A.J., Akrami, M., Mehrzad, J., Bardania, H., 2020. Recent progress in biomedical applications of RGD-based ligand: from precise cancer theranostics to biomaterial engineering: a systematic review. J. Biomed. Mater. Res. 108, 839–850. https://doi.org/10.1002/jbm.a.36862.

Arosio, D., Belvisi, L., Colombo, L., Colombo, M., Invernizzi, D., Manzoni, L., Potenza, D., Serra, M., Castorina, M., Pisano, C., Scolastico, C., 2008. A potent integrin antagonist from a small library of cyclic RGD pentapeptide mimics including benzyl-substituted azabicycloalkane amino acids. ChemMedChem 3, 1589–1603. https://doi.org/10.1002/cmdc.200800143.

Arosio, D., Casagrande, C., 2016. Advancement in integrin facilitated drug delivery. Adv. Drug Deliv. Rev. 97, 111–143. https://doi.org/10.1016/j.addr.2015.12.001.

Bari, E., Serra, M., Paolillo, M., Bernardi, E., Tengattini, S., Piccinini, F., Lanni, C., Sorlini, M., Bisbano, G., Calleri, E., Torre, M.L., Perteghella, S., 2021. Silk fibroin nanoparticle functionalization with arg-gly-asp cyclopentapeptide promotes active targeting for tumor site-specific delivery. Cancers 13, 1185. https://doi.org/10.3390/cancers13051185.

Battistini, L., Bugatti, K., Sartori, A., Curti, C., Zanardi, F., 2021. RGD peptide-drug conjugates as effective dual targeting platforms: recent advances. Eur. J. Org. Chem. 2021, 2506–2528. https://doi.org/10.1002/ejoc.202100240.

Bianchini, G., Balko, J.M., Mayer, I.A., Sanders, M.E., Gianni, L., 2016. Triple-negative breast cancer: challenges and opportunities of a heterogeneous disease. Nat. Rev. Clin. Oncol. 13, 674–690. https://doi.org/10.1038/nrclinonc.2016.66.

Bray, F., Ferlay, J., Soerjomataram, I., Siegel, R.L., Torre, L.A., Jemal, A., 2018. Global cancer statistics 2018: GLOBOCAN estimates of incidence and mortality worldwide for 36 cancers in 185 countries. CA Cancer J. Clin. 68, 394–424. https://doi.org/10.3322/caac.21492.

Denard, B., Jiang, S., Peng, Y., Ye, J., 2018. CREB3L1 as a potential biomarker predicting response of triple negative breast cancer to doxorubicin-based chemotherapy. BMC Cancer 18, 813. https://doi.org/10.1186/s12885-018-4724-8.

Fritze, A., Hens, F., Kimpfler, A., Schubert, R., Peschka-Süss, R., 2006. Remote loading of doxorubicin into liposomes driven by a transmembrane phosphate gradient. Biochim. Biophys. Acta BBA Biomembr. 1758, 1633–1640. https://doi.org/10.1016/j.bbamem.2006.05.028.

Fujisawa, T., Rubin, B., Suzuki, A., Patel, P.S., Gahl, W.A., Joshi, B.H., Puri, R.K., 2012. Cysteamine suppresses invasion, metastasis and prolongs survival by inhibiting matrix metalloproteinases in a mouse model of human pancreatic cancer. PLOS ONE 7, e34437. https://doi.org/10.1371/journal.pone.0034437.

Gomes, A.J., Barbougli, P.A., Espreafico, E.M., Tfouni, E., 2008. trans-[Ru(NO)(NH3)4(py)](BF4)3·H2O encapsulated in PLGA microparticles for delivery of nitric oxide to B16-F10 cells: cytotoxicity and phototoxicity. J. Inorg. Biochem. 102, 757–766. https://doi.org/10.1016/j.jinorgbio.2007.11.012.

Gomes, A.J., Espreafico, E.M., Tfouni, E., 2013. Trans-[Ru(NO)Cl(cyclam)](PF6)2 and [Ru(NO)(Hedta)] incorporated in PLGA nanoparticles for the delivery of nitric oxide to B16-F10 cells: cytotoxicity and phototoxicity. Mol. Pharm. 10, 3544–3554. https://doi.org/10.1021/mp3005534.

Hai, J., Zhu, C.Q., Bandarchi, B., Wang, Y.H., Navab, R., Shepherd, F.A., Jurisica, I., Tsao, M.S., 2012. L1 cell adhesion molecule promotes tumorigenicity and metastatic potential in non–Small Cell lung cancer. Clin. Cancer Res. 18, 1914–1924. https://doi.org/10.1158/1078-0432.CCR-11-2893.

Hill, B.S., Sarnella, A., Capasso, D., Comegna, D., Del Gatto, A., Gramanzini, M., Albanese, S., Saviano, M., Zaccaro, L., Zannetti, A., 2019. Therapeutic potential of a novel αvβ3 antagonist to hamper the aggressiveness of mesenchymal triple negative breast cancer sub-type. Cancers 11, 139. https://doi.org/10.3390/cancers11020139.

Keller, F., Rudolf, R., Hafner, M., 2019. Towards optimized breast cancer 3D spheroid mono- and co-culture models for pharmacological research and screening. J. Cell. Biotechnol. 5, 89–101. https://doi.org/10.3233/JCB-199001.

Kranz, H., Bodmeier, R., 2007. A novel *in situ* forming drug delivery system for controlled parenteral drug delivery. Int. J. Pharm. 332, 107–114. https://doi.org/10.1016/j.ijpharm.2006.09.033.

Lao, J., Madani, J., Puértolas, T., Alvarez, M., Hernández, A., Pazo-Cid, R., Artal, A., Antón Torres, A., 2013. Liposomal doxorubicin in the treatment of breast cancer patients: a review. J. Drug Deliv. 2013, 456409. https://doi.org/10.1155/2013/456409.

Lazaro-Carrillo, A., Filice, M., Guillén, M.J., Amaro, R., Viñambres, M., Tabero, A., Paredes, K.O., Villanueva, A., Calvo, P., del Puerto Morales, M., Marciello, M., 2020. Tailor-made PEG coated iron oxide nanoparticles as contrast agents for long lasting magnetic resonance molecular imaging of solid cancers. Mater. Sci. Eng. C 107, 110262. https://doi.org/10.1016/j.msec.2019.110262.

Lecomte, N., Njardarson, J.T., Nagorny, P., Yang, G., Downey, R., Ouerfelli, O., Moore, M.A.S., Danishefsky, S.J., 2011. Emergence of potent inhibitors of metastasis in lung cancer via syntheses based on migrastatin. Proc. Natl. Acad. Sci. 108, 15074–15078. https://doi.org/10.1073/pnas.1015247108.

Lee, K.L., Kuo, Y.C., Ho, Y.S., Huang, Y.H., 2019. Triple-negative breast cancer: current understanding and future therapeutic breakthrough targeting cancer stemness. Cancers 11, 1334. https://doi.org/10.3390/cancers11091334.

Li, Y., Drabsch, Y., Pujuguet, P., Ren, J., van Laar, T., Zhang, L., van Dam, H., Clément-Lacroix, P., ten Dijke, P., 2015. Genetic depletion and pharmacological targeting of αv integrin in breast cancer cells impairs metastasis in zebrafish and mouse xenograft models. Breast Cancer Res. 17, 28. https://doi.org/10.1186/s13058-015-0537-8.

Liedtke, C., Mazouni, C., Hess, K.R., André, F., Tordai, A., Mejia, J.A., Symmans, W.F., Gonzalez-Angulo, A.M., Hennessy, B., Green, M., Cristofanilli, M., Hortobagyi, G.N., Pusztai, L., 2008. Response to neoadjuvant therapy and long-term survival in patients with triple-negative breast cancer. J. Clin. Oncol. 26, 1275–1281. https://doi.org/10.1200/JCO.2007.14.4147.

Luengo Morato, Y., Ovejero Paredes, K., Lozano Chamizo, L., Marciello, M., Filice, M., 2021. Recent advances in multimodal molecular imaging of cancer mediated by hybrid magnetic nanoparticles. Polymers 13, 2989. https://doi.org/10.3390/polym13172989.

Marciello, M., Pellico, J., Fernandez-Barahona, I., Herranz, F., Ruiz-Cabello, J., Filice, M., 2016. Recent advances in the preparation and application of multifunctional iron oxide and liposome-based nanosystems for multimodal diagnosis and therapy. Interface Focus 6, 20160055. https://doi.org/10.1098/rsfs.2016.0055.

Martin, M., Ramos-Medina, R., Bernat, R., García-Saenz, J.A., del Monte-Millan, M., Alvarez, E., Cebollero, M., Moreno, F., Gonzalez-Haba, E., Bueno, O., Romero, P., Massarrah, T., Echavarria, I., Jerez, Y., Herrero, B., Gonzalez del Val, R., Lobato, N., Rincon, P., Palomero, M.I., Marquez-Rodas, I., Lizarraga, S., Asensio, F., Lopez-Tarruella, S., 2021. Activity of docetaxel, carboplatin, and doxorubicin in patient-derived triple-negative breast cancer xenografts. Sci. Rep. 11, 7064. https://doi.org/10.1038/s41598-021-85962-4.

Mas-Moruno, C., Rechenmacher, F., Kessler, H., 2010. Cilengitide: the first anti-angiogenic small molecule drug candidate design, synthesis and clinical evaluation. Anticancer Agents Med. Chem. 10, 753–768. https://doi.org/10.2174/187152010794728639.

Mbua, N.E., Guo, J., Wolfert, M.A., Steet, R., Boons, G.J., 2011. Strain-promoted alkyne-azide cycloadditions (SPAAC) reveal new features of glycoconjugate biosynthesis. Chembiochem Eur. J. Chem. Biol. 12, 1912–1921. https://doi.org/10.1002/cbic.201100117.

Mustacchi, G., De Laurentiis, M., 2015. The role of taxanes in triple-negative breast cancer: literature review. Drug Des. Dev. Ther. 9, 4303–4318. https://doi.org/10.2147/DDDT.S86105.

Nogueira, E., Gomes, A.C., Preto, A., Cavaco-Paulo, A., 2015. Design of liposomal formulations for cell targeting. Colloids Surf. B Biointerfaces 136, 514–526. https://doi.org/10.1016/j.colsurfb.2015.09.034.

Ovejero Paredes, K., Díaz-García, D., García-Almodóvar, V., Lozano Chamizo, L., Marciello, M., Díaz-Sánchez, M., Prashar, S., Gómez-Ruiz, S., Filice, M., 2020. Multifunctional silica-based nanoparticles with controlled release of organotin metallodrug for targeted theranosis of breast cancer. Cancers 12, 187. https://doi.org/10.3390/cancers12010187.

Ovejero-Paredes, K., Díaz-García, D., Mena-Palomo, I., Marciello, M., Lozano-Chamizo, L., Morato, Y.L., Prashar, S., Gómez-Ruiz, S., Filice, M., 2022. Synthesis of a theranostic platform based on fibrous silica nanoparticles for the enhanced treatment of triple-negative breast cancer promoted by a combination of chemotherapeutic agents. Biomater. Adv. 137, 212823. https://doi.org/10.1016/j.bioadv.2022.212823.

Paolillo, M., Galiazzo, M.C., Daga, A., Ciusani, E., Serra, M., Colombo, L., Schinelli, S., 2018. An RGD small-molecule integrin antagonist induces detachment-mediated anoikis in glioma cancer stem cells. Int. J. Oncol. 53, 2683–2694. https://doi.org/10.3892/ijo.2018.4583.

Pirota, V., Bisbano, G., Serra, M., Torre, M.L., Doria, F., Bari, E., Paolillo, M., 2023. cRGD-functionalized silk fibroin nanoparticles: a strategy for cancer treatment with a potent unselective naphthalene diimide derivative. Cancers 15, 1725. https://doi.org/10.3390/cancers15061725.

Plati, J., Bucur, O., Khosravi-Far, R., 2011. Apoptotic cell signaling in cancer progression and therapy. Integr. Biol. Quant. Biosci. Nano Macro 3, 279–296. https://doi.org/10.1039/c0ib00144a.

Ramadan, W.S., Vazhappilly, C.G., Saleh, E.M., Menon, V., AlAzawi, A.M., El-Serafi, A.T., Mansour, W., El-Awady, R., 2018. Interplay between epigenetics, expression of estrogen receptor- α, HER2/ERBB2 and sensitivity of triple negative breast cancer cells to hormonal therapy. Cancers 11, 13. https://doi.org/10.3390/cancers11010013.

Russo, M.A., Paolillo, M., Sanchez-Hernandez, Y., Curti, D., Ciusani, E., Serra, M., Colombo, L., Schinelli, S., 2012. A small-molecule RGD-integrin antagonist inhibits cell adhesion, cell migration and induces anoikis in glioblastoma cells. Int. J. Oncol. 42, 83. https://doi.org/10.3892/ijo.2012.1708.

Saiz, M.L., Lozano-Chamizo, L., Florez, A.B., Marciello, M., Diaz-Bulnes, P., Corte-Iglesias, V., Bernet, C.R., Rodrigues-Diez, R.R., Martin-Martin, C., Rodriguez-Santamaria, M., Fernandez-Vega, I., Rodriguez, R.M., Diaz-Corte, C., Suarez-Alvarez, B., Filice, M., Lopez-Larrea, C., 2024. BET inhibitor nanotherapy halts kidney damage and reduces chronic kidney disease progression after ischemia-reperfusion injury. Biomed. Pharmacother. Biomed. Pharmacother. 174, 116492. https://doi.org/10.1016/j.biopha.2024.116492.

Sánchez, A., Ovejero Paredes, K., Ruiz-Cabello, J., Martínez-Ruíz, P., Pingarrón, J.M., Villalonga, R., Filice, M., 2018. Hybrid decorated core@Shell Janus nanoparticles as a flexible platform for targeted multimodal molecular bioimaging of cancer. ACS Appl. Mater. Interfaces 10, 31032–31043. https://doi.org/10.1021/acsami.8b10452.

Sanchez-Collado, J., Lopez, J.J., Jardin, I., Camello, P.J., Falcon, D., Regodon, S., Salido, G.M., Smani, T., Rosado, J.A., 2019. Adenylyl cyclase type 8 overexpression impairs phosphorylation-dependent Orai1 inactivation and promotes migration in MDA-MB-231 breast cancer cells. Cancers 11, 1624. https://doi.org/10.3390/cancers11111624.

Seo, T.S., Li, Z., Ruparel, H., Ju, J., 2003. Click chemistry to construct fluorescent oligonucleotides for DNA sequencing. J. Org. Chem. 68, 609–612. https://doi.org/10.1021/jo026615r.

Serra, M., Peviani, E.G., Bernardi, E., Colombo, L., 2017. Synthesis of variously functionalized azabicycloalkane scaffolds by domino metathesis reactions. J. Org. Chem. 82, 11091–11101. https://doi.org/10.1021/acs.joc.7b02047.

Serra, M., Rubes, D., Schinelli, S., Paolillo, M., 2023a. Small molecules against metastatic tumors: concrete perspectives and shattered dreams. Cancers 15, 4173. https://doi.org/10.3390/cancers15164173.

Serra, M., Terreni, M., Bernardi, E., Colombo, L., 2023b. Synthesis of functionalized proline-derived azabicycloalkane amino acids and their applications in drug discovery: recent advances. Eur. J. Org. Chem. 26, e202201394. https://doi.org/10.1002/ejoc.202201394.

Shah, S., Dhawan, V., Holm, R., Nagarsenker, M.S., Perrie, Y., 2020. Liposomes: advancements and innovation in the manufacturing process. Adv. Drug Deliv. Rev. 154–155, 102–122. https://doi.org/10.1016/j.addr.2020.07.002.

Shepherd, S.J., Warzecha, C.C., Yadavali, S., El-Mayta, R., Alameh, M.G., Wang, L., Weissman, D., Wilson, J.M., Issadore, D., Mitchell, M.J., 2021. Scalable mRNA and siRNA lipid nanoparticle production using a parallelized microfluidic device. Nano Lett. 21, 5671–5680. https://doi.org/10.1021/acs.nanolett.1c01353.

Stewart, J.C.M., 1980. Colorimetric determination of phospholipids with ammonium ferrothiocyanate. Anal. Biochem. 104, 10–14. https://doi.org/10.1016/0003-2697(80)90269-9.

Stupp, R., Hegi, M.E., Gorlia, T., Erridge, S.C., Perry, J., Hong, Y.K., Aldape, K.D., Lhermitte, B., Pietsch, T., Grujicic, D., Steinbach, J.P., Wick, W., Tarnawski, R., Nam, D.H., Hau, P., Weyerbrock, A., Taphoorn, M.J.B., Shen, C.C., Rao, N., Thurzo, L., Herrlinger, U., Gupta, T., Kortmann, R.D., Adamska, K., McBain, C., Brandes, A.A., Tonn, J.C., Schnell, O., Wiegel, T., Kim, C.Y., Nabors, L.B., Reardon, D.A., van den Bent, M.J., Hicking, C., Markivskyy, A., Picard, M., Weller, M., European Organisation for Research and Treatment of Cancer (EORTC), Canadian Brain Tumor Consortium, CENTRIC study Team, 2014. Cilengitide combined with standard treatment for patients with newly diagnosed glioblastoma with methylated MGMT promoter (CENTRIC EORTC 26071-22072 study): a multicentre, randomised, open-label, phase 3 trial. Lancet Oncol. 15, 1100–1108. https://doi.org/10.1016/S1470-2045(14)70379-1.

Tenchov, R., Bird, R., Curtze, A.E., Zhou, Q., 2021. Lipid nanoparticles–from liposomes to mRNA vaccine delivery, a landscape of research diversity and advancement. ACS Nano 15, 16982–17015. https://doi.org/10.1021/acsnano.1c04996.

Thomas, E.S., Gomez, H.L., Li, R.K., Chung, H.C., Fein, L.E., Chan, V.F., Jassem, J., Pivot, X.B., Klimovsky, J.V., De Mendoza, F.H., Xu, B., Campone, M., Lerzo, G.L., Peck, R.A., Mukhopadhyay, P., Vahdat, L.T., Roché, H.H., 2007. Ixabepilone plus Capecitabine for metastatic breast cancer progressing after anthracycline and taxane treatment. J. Clin. Oncol. 25, 5210–5217. https://doi.org/10.1200/JCO.2007.12.6557.

Thorn, C.F., Oshiro, C., Marsh, S., Hernandez-Boussard, T., McLeod, H., Klein, T.E., Altman, R.B., 2011. Doxorubicin pathways: pharmacodynamics and adverse effects. Pharmacogenet. Genom. 21, 440–446. https://doi.org/10.1097/FPC.0b013e32833ffb56.

Tian, H., Zhang, T., Qin, S., Huang, Z., Zhou, L., Shi, J., Nice, E.C., Xie, N., Huang, C., Shen, Z., 2022. Enhancing the therapeutic efficacy of nanoparticles for cancer treatment using versatile targeted strategies. J. Hematol. Oncol. 15, 132. https://doi.org/10.1186/s13045-022-01320-5.

Wang, X., Yang, L., Chen, Z.G., Shin, D.M., 2008. Application of nanotechnology in cancer therapy and imaging. CA Cancer J. Clin. 58, 97–110. https://doi.org/10.3322/CA.2007.0003.

Wei, G., Xiao, S., Si, D., Liu, C., 2008. Improved HPLC method for doxorubicin quantification in rat plasma to study the pharmacokinetics of micelle-encapsulated and liposome-encapsulated doxorubicin formulations. Biomed. Chromatogr. BMC 22, 1252–1258. https://doi.org/10.1002/bmc.1054.

Won, K.A., Spruck, C., 2020. Triple-negative breast cancer therapy: current and future perspectives (Review). Int. J. Oncol. 57, 1245–1261. https://doi.org/10.3892/ijo.2020.5135.

Wu, P.H., Onodera, Y., Ichikawa, Y., Rankin, E.B., Giaccia, A.J., Watanabe, Y., Qian, W., Hashimoto, T., Shirato, H., Nam, J.M., 2017. Targeting integrins with RGD-conjugated gold nanoparticles in radiotherapy decreases the invasive activity of breast cancer cells. Int. J. Nanomed. 12, 5069–5085. https://doi.org/10.2147/IJN.S137833.

Zahraei, M., Marciello, M., Lazaro-Carrillo, A., Villanueva, A., Herranz, F., Talelli, M., Costo, R., Monshi, A., Shahbazi-Gahrouei, D., Amirnasr, M., Behdadfar, B., Morales, M.P., 2016. Versatile theranostics agents designed by coating ferrite nanoparticles with biocompatible polymers. Nanotechnology 27, 255702. https://doi.org/10.1088/0957-4484/27/25/255702.

Zhang, G., Sun, J., 2021. Lipid in chips: a brief review of liposomes formation by microfluidics. Int. J. Nanomed. 16, 7391–7416. https://doi.org/10.2147/IJN.S331639.